

# **Our Research activities in India and at JINR**

**Ajay Kr. Tyagi**  
**Department of Physics**  
**Banaras Hindu University, Varanasi**

# Plan of talk

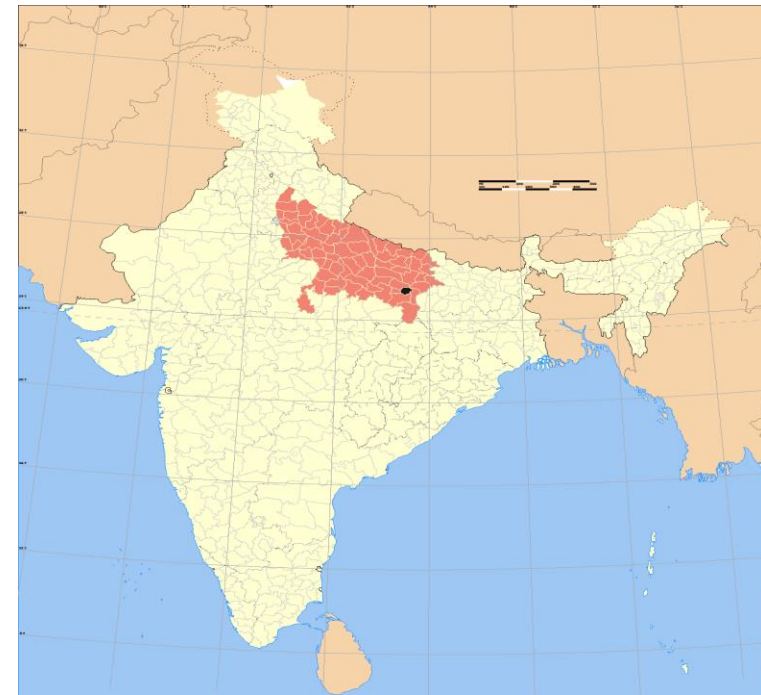
- 1. Who we are**
- 2. BHU and JINR**
- 2. What we are doing at BHU**
- 3. Possible research activities at JINR, Dubna and in India**

## Banaras Hindu University, Varanasi, India

- ❖ Varanasi is located in the middle-Ganges valley in the southeastern part of the state of Uttar Pradesh, lies on the left bank of the river. It is 692 kilometers (430 mi) to the southeast of India's capital New Delhi.
- ❖ Banaras Hindu University was founded in 1916 with area 1300 acres (5.3 Km<sup>2</sup>). It is the largest residential university of India having more than 30,000 students, 1700 faculty members and 144 departments.
- ❖ A large number of students from U.S.A, Europe, Asia, Middle East, Africa etc., come to BHU.

## Department of Physics, BHU

- ❖ The Department of Physics is having 65 faculties with 6 specializations and more than 160 PhD students.



**We are having a vibrant group of seven PhD students from different parts of India and working on very interesting Nuclear Physics problems and publishing their work in highly repute research journals.**

**1. Heavy Ion fusion–fission dynamics by using 15 UD Pelletron at IUAC, New Delhi and BARC-TIFR Pelletron, Mumbai**

**2. Neutron scattering experiments at BARC, Mumbai, India**

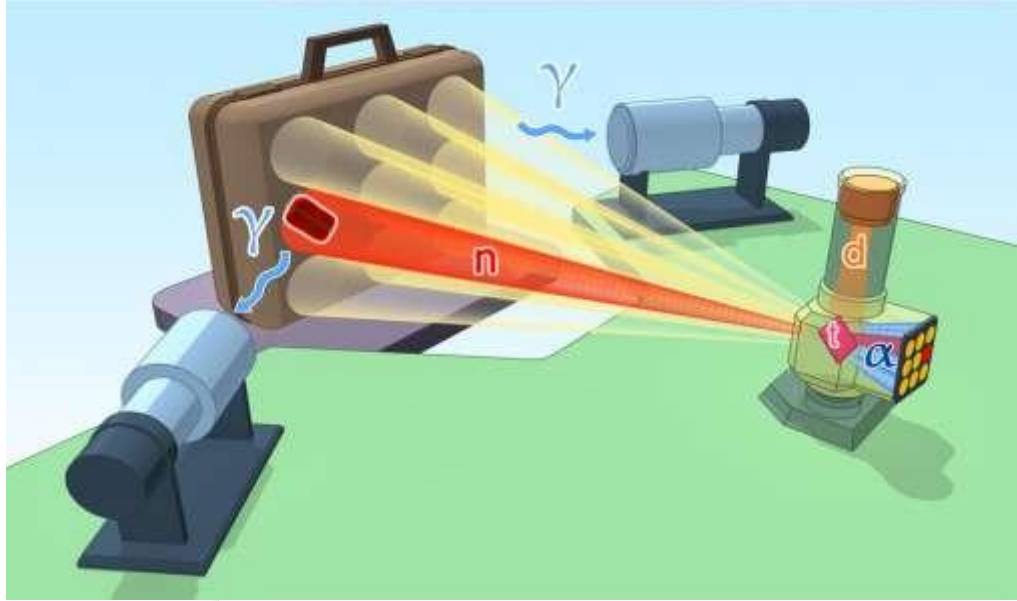
**3. Surrogate reaction dynamics by using BARC-TIFR, Pelletron facility Mumbai**

**4. Alpha and Proton scattering experiments at Variable Energy Cyclotron (VECC), Kolkata**

**5. Neural networks and Nuclear Physics**

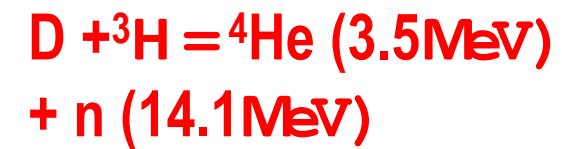


## Tagged Neutrons Method – TNM



### Main components:

- Neutron generator
- Position sensitive detector of  $\alpha$ -particles
- Detectors of  $\gamma$ -rays / neutrons



# Aims of the project

1. Using tagged neutron beams for experimental investigations in the field of fundamental Nuclear Physics.
2. Investigation of reactions  $(n,n',\gamma)$  using the tagged neutrons method.
3. Investigation of reactions  $(n,2n')$ ,  $(n,n')$  using the tagged neutron method.
4. Development of the tagged neutron method for identification of a wider range of elements and substances.
5. Development of a database on reaction cross sections for interaction of neutrons with energy 14.1 MeV with nuclei and on the characteristic gamma lines.

**For high energy gamma rays spectroscopy BGOs (Bismuth Germanium Oxides) detectors are widely used due to the high atomic number of Bismuth (83) and its high density which make him the most efficient gamma-absorber.**



**Left Side View**



**Right Side View**

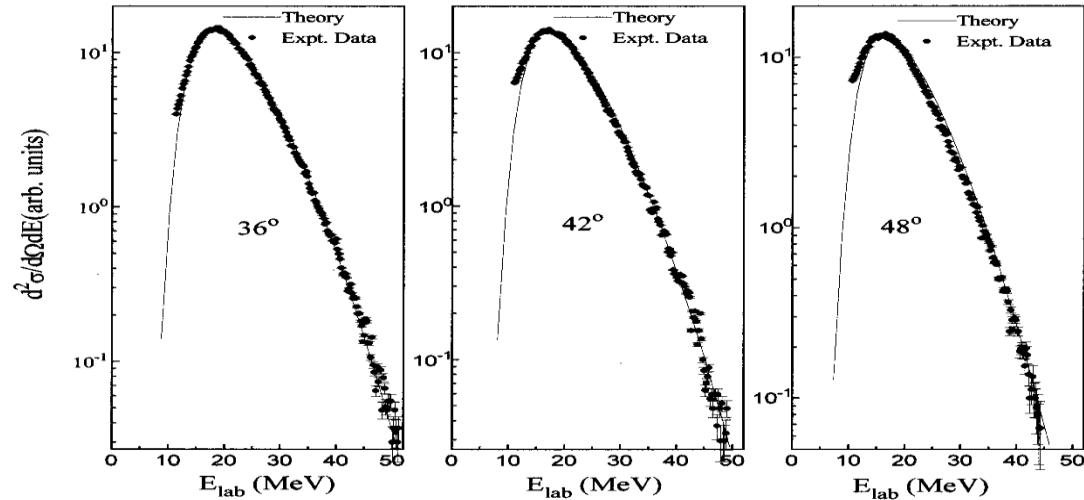
**Fig: A multi detector system “Romasha” formed of 18 BGO detectors.**

**Each side we have 9 BGO detectors at a distance of 75cm and at angle of 14degree from the centre of neutron source.**

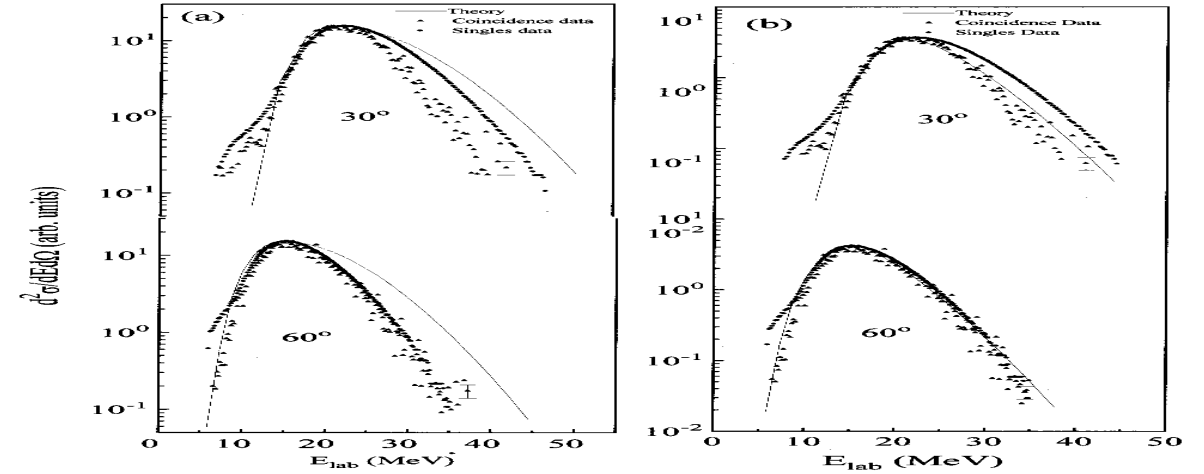
## Some pictures of the work under BHU-Russian Collaboration



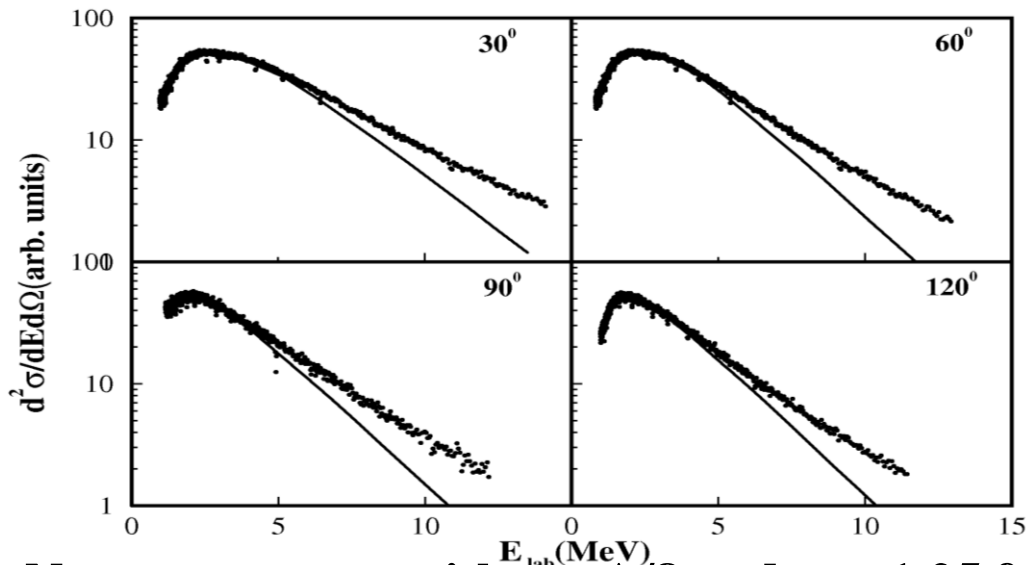
# Study of heavy ion fusion dynamics



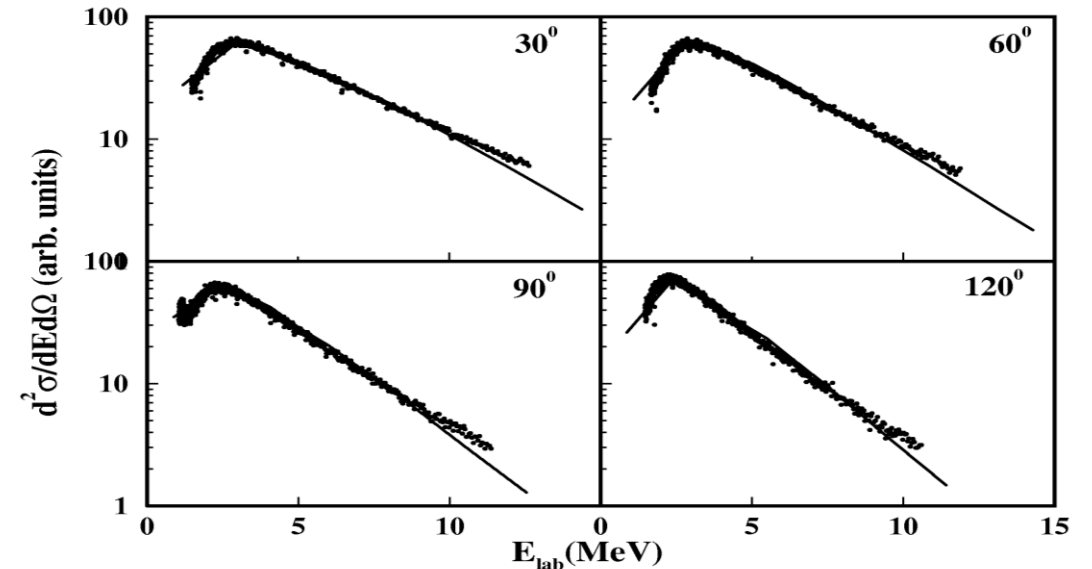
$\alpha$ -spectra with  $\ell_{\max} = 48\hbar$  for  $^{16}\text{O} + ^{54}\text{Fe}$  at 110 MeV.



$\alpha$ -spectra for  $^{28}\text{Si} + ^{51}\text{V}$ . (a)  $\ell_{\max} = 56\hbar$  (b)  $\ell_{\max} = 30\hbar$



Neutron spectra with  $a = A/8$  and  $r_0 = 1.25$  for  $^{31}\text{P} + ^{45}\text{Sc}$  with  $\ell_{\max} = 39\hbar$  at  $E_{\text{lab}} = 112$  MeV.



Neutron spectra using  $r_0 = 1.25$  and  $a = A/8$  for  $^{12}\text{C} + ^{64}\text{Zn}$  with  $\ell_{\max} = 39\hbar$  at  $E_{\text{lab}} = 85$  MeV.

# Effect of energy variation on the dissipative evolution of the system in heavy-ion fusion reactions

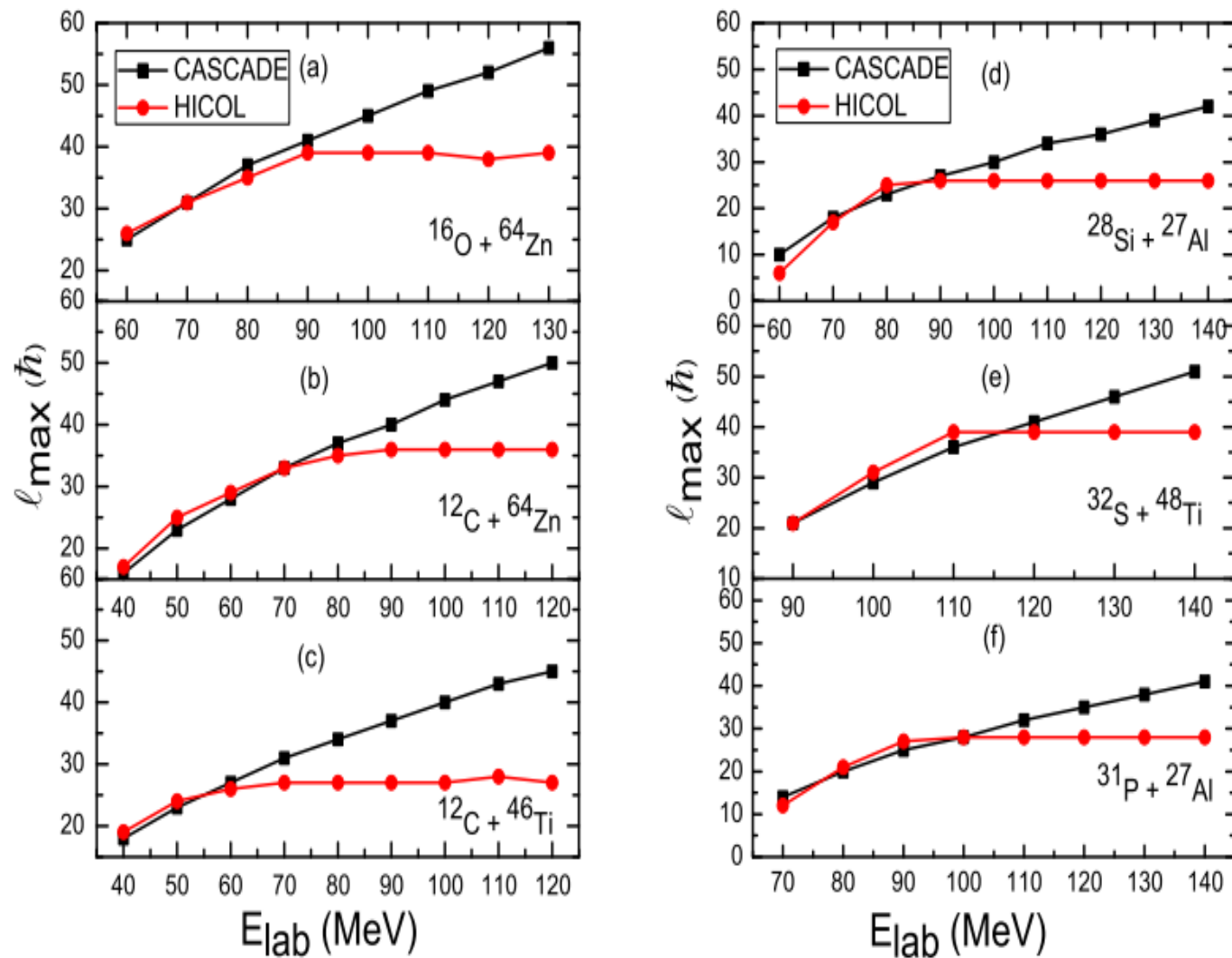
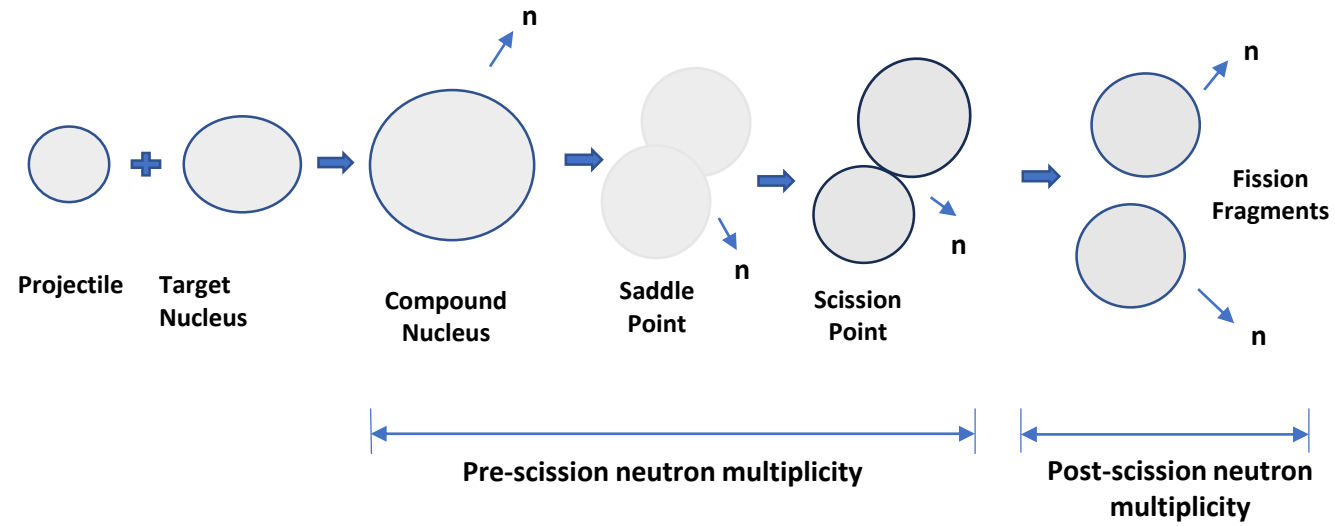


FIG. 4. Variation of angular momentum  $l_{\max}$  with respect to incident energy  $E_{\text{lab}}$  for asymmetric systems (a)–(c) and symmetric systems (d)–(f).

N.K. Rai and Ajay Kumar, Phys. Rev. C **98**, 024626 (2018).

- Dissipation in the entrance channel increases with the projectile energy and causes the angular momentum hindrance in both the symmetric and asymmetric systems at the higher energy.
- The dissipative behavior of the fusing nuclei also depends on the entrance channel parameters.
- We observed that with increasing value of mass asymmetry angular momentum hindrance decreases linearly, and angular momentum hindrance increases linearly with an increase in the coulomb interaction term ( $Z_p Z_t$ ).



## Decay of fission-fragments from Compound Nucleus

# Measurement of neutrons multiplicity to investigate the role of entrance channel parameters on the nuclear dissipation

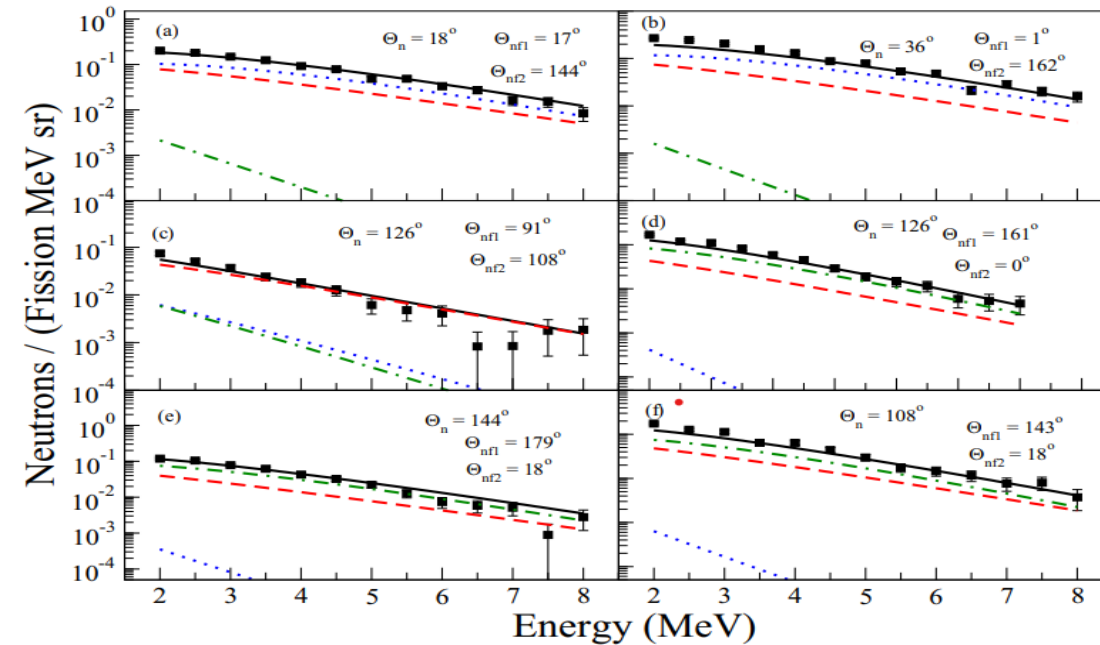
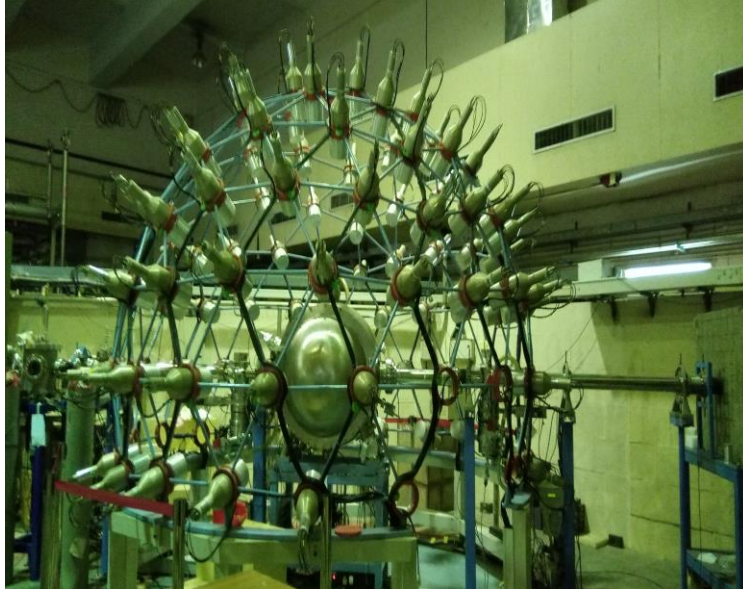
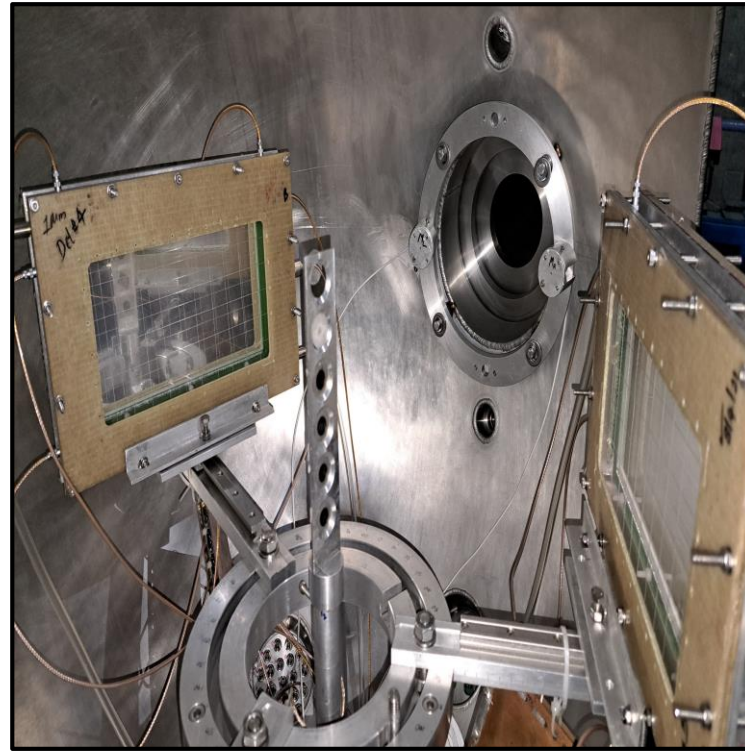
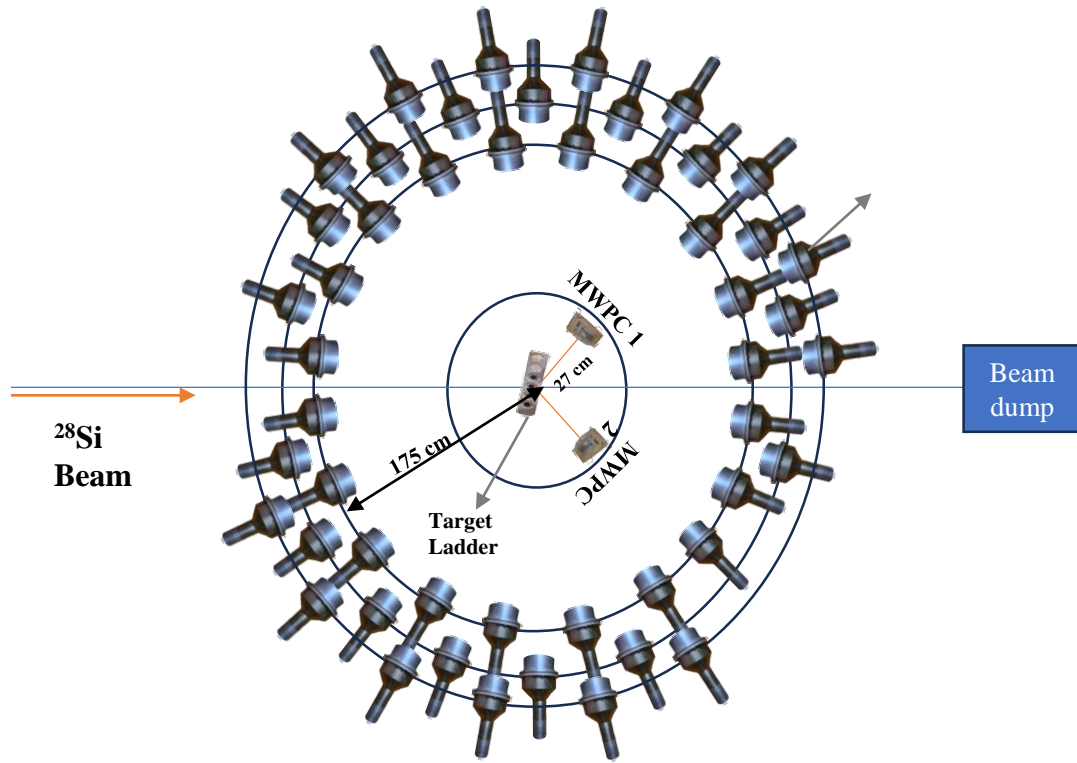


FIG. 1. Neutron multiplicity spectra (filled squares) at various angles for the reaction  $^{18}\text{O} + ^{186}\text{W}$  at  $E_{\text{lab}} = 106.51$  MeV along with the fits for the pre-scission (dashed lines) and post-scission contributions from the one fragment (dotted lines) and that from the other (dotted-dash lines) are shown. Here, the solid black line represents the total contribution.

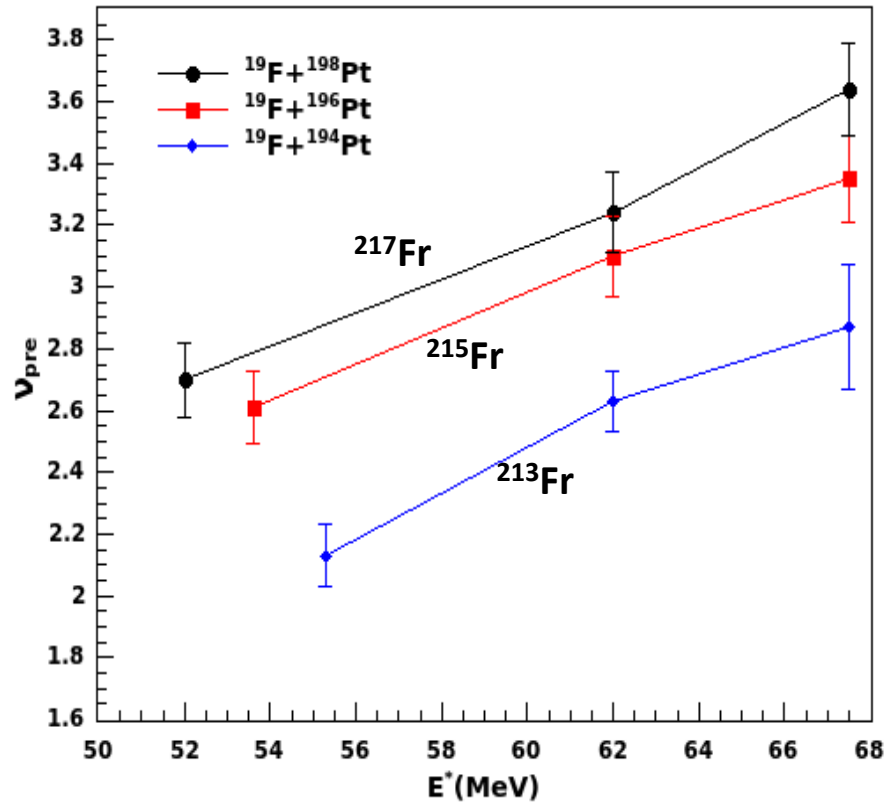
Measured the pre- and post-scission neutron multiplicity for  $^{18}\text{O} + ^{186}\text{W}$  and compared with  $^{16}\text{O} + ^{181}\text{Ta}$ , existing in the literature. Nuclear dissipation decreases with the increasing value of the entrance channel mass asymmetry. In the present case, it was also verified that nuclear dissipation increases with the increasing value of the Coulomb factor  $ZPZT$  as mentioned in our theoretical work (PRC 2018).

Ajay Kumar Tyagi et al, Phys. Rev. C **100**, 014614 (2019).



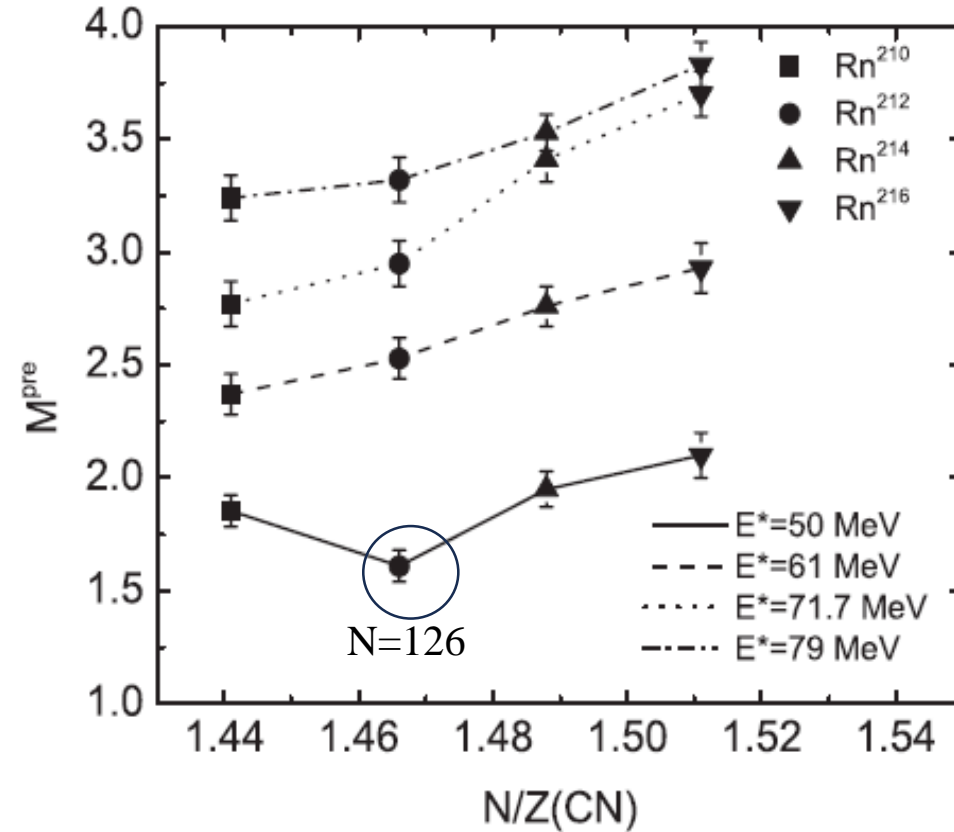
Inside view of NAND scattering chamber

# How We Were Motivated for the Present Work



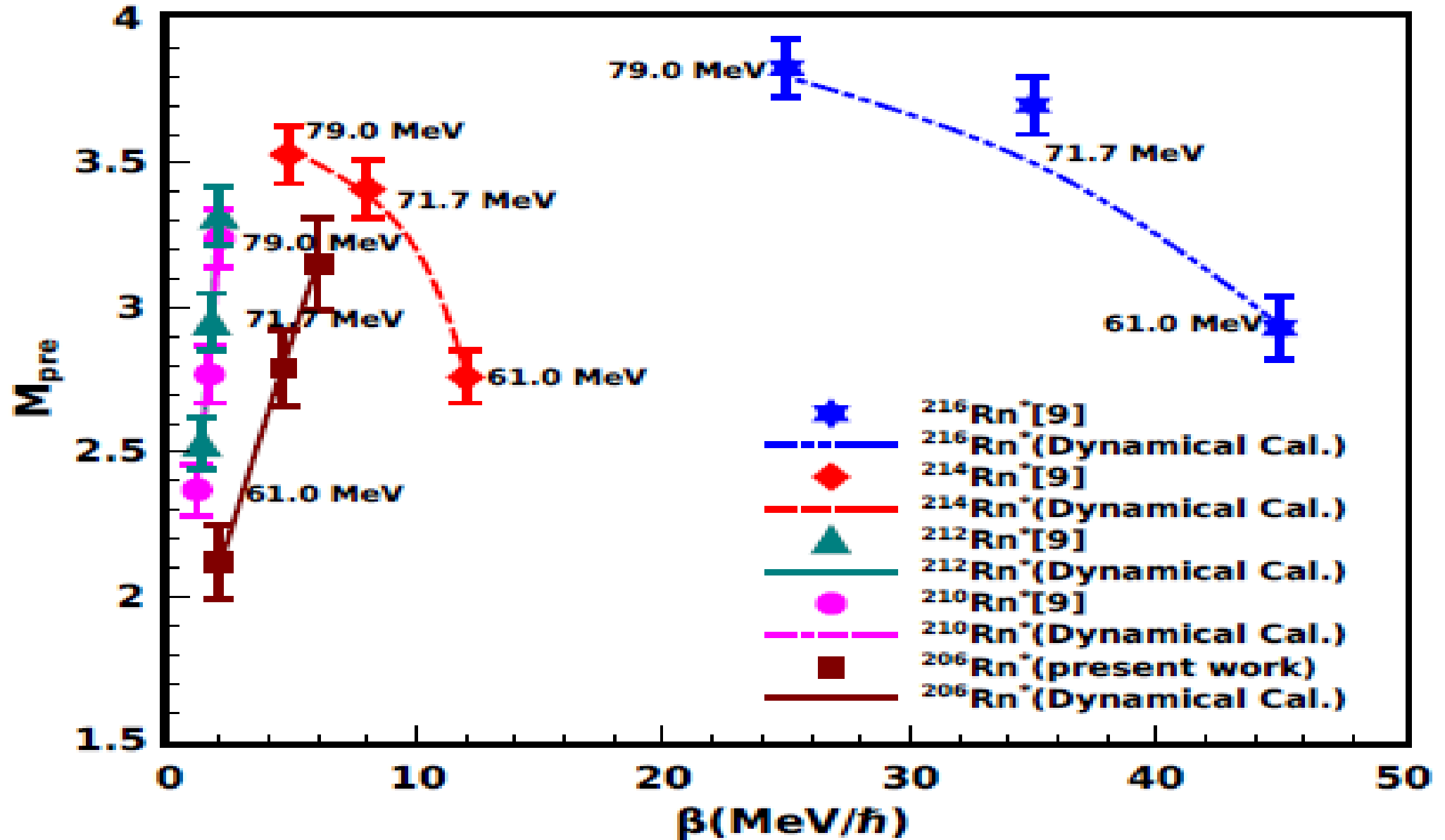
V. Singh *et. al.* PRC **86**, 014609 (2012)

Shell closure effect seen for  $^{213}\text{Fr}$  (N=126) compound nucleus.

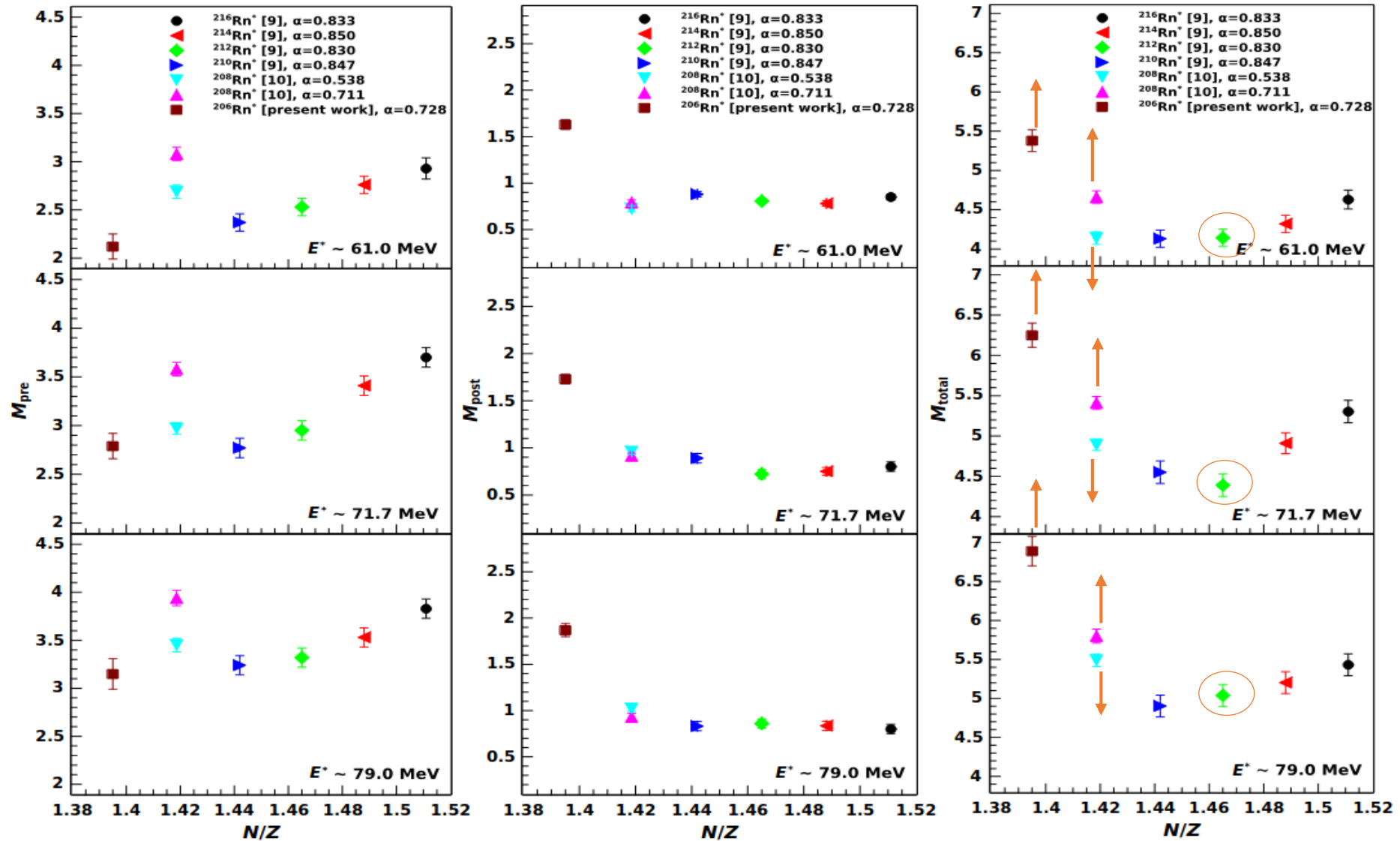


Rohit Sandal *et. al.* PRC **87**, 014604 (2013)

➤ N/Z value does not affect dissipation specifically.



Variation in  $\beta$  w.r.t  $M_{pre}$  for compound nucleus  $^{206-216}\text{Rn}^*$  w.r.t. excitation energy.  
 $30,28\text{Si}+178\text{Hf}=208,206\text{Rn}$ ,  $16,18\text{O}+194,198\text{Pt}=210,12,14,16\text{Rn}$



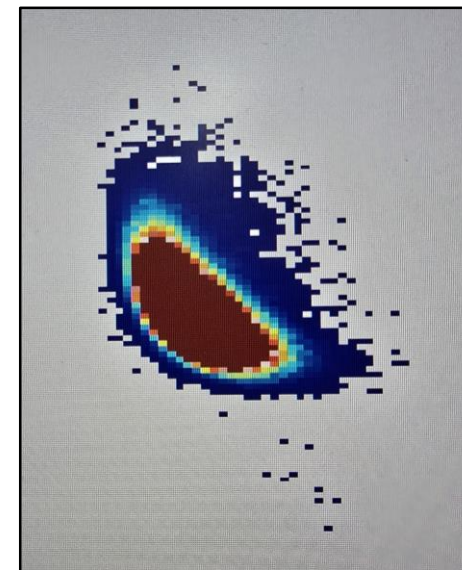
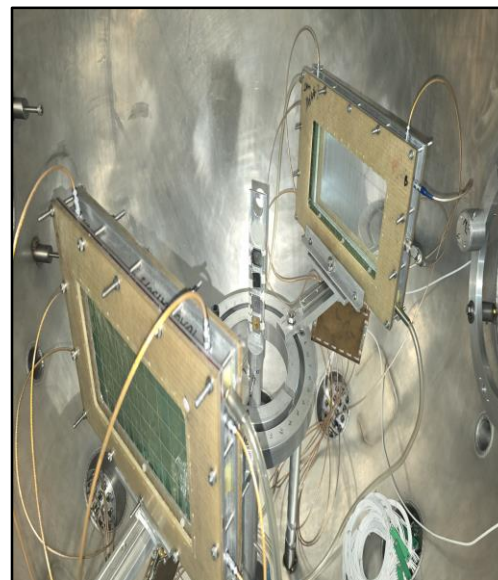
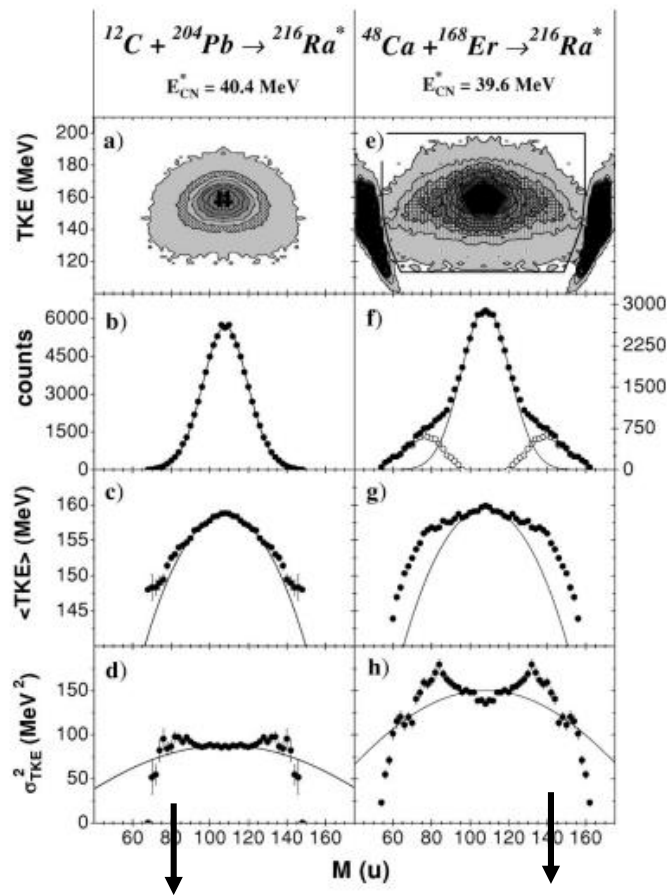
➤ Variation of  $M_{\text{pre}}$  (left),  $M_{\text{post}}$  (center), and  $M_{\text{total}}$  (right) with respect to the  $N/Z$  ratio for compound nuclei  $^{206,208,210,212,214,216}\text{Rn}$  at excitation energies of 61.0, 71.7, and 79.0 MeV.

## Conclusion

- ❑ Below shell closure, dissipation increases with rise in excitation energy, around shell remains stable, while beyond shell closure dissipation gradually decreases as excitation energy increases..
- ❑  $M_{\text{total}}$  decreases around shell closure compound nuclei, while increases when move away from shell closure either side.
- ❑ More experimental data near shell closure ( $^{208}\text{Pb}$ ,  $^{209}\text{Bi}$ , and  $^{211}\text{At}$ ) in the pre-actinide region are required to see this effects in fission dynamics.
- ❑ Further investigations are necessary in the mass region above  $A_{\text{CN}}=220$  to examine the influence of shell closure. To achieve this, higher-mass projectile beams such as  $^{48}\text{Ca}$  are required, which are currently unavailable in India. Therefore, such experiments can be planned to be conducted at JINR, Dubna.

# To study the impact of entrance channel through fission fragment mass distribution

CA. Yu. Chizhov et al., Phys. Rev. C 67, 011603(R) (2003).



- Fusion-Fission
- No significant contribution from asymmetric fission (~1.5%)
- Quasi-fission
- Large contribution (~30%) of asymmetric fission mode

## Mass Asymmetry

Mass Asymmetry,  $\alpha = [(A_T - A_P)/(A_T + A_P)]$

where,  $T$  is Target,  $P$  is Projectile,  $A$  is the mass number

Reaction	Mass Asymmetry	Businaro-Gallone mass asymmetry ( $\alpha_{BG}$ )
$^{14}\text{N} + ^{209}\text{Bi} \rightarrow ^{223}\text{Th}$	0.8744	0.8715
$^{16}\text{O} + ^{207}\text{Pb} \rightarrow ^{223}\text{Th}$	0.8565	

## Product of Charges

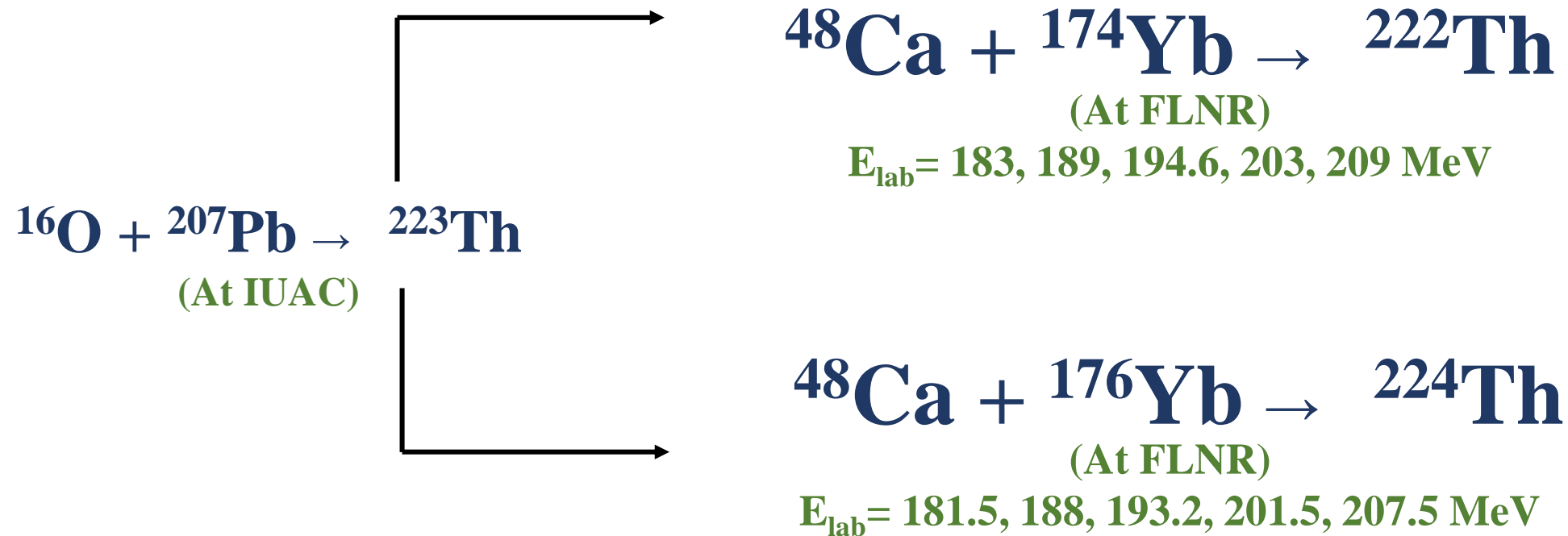
Reaction	$Z_P Z_T$
$^{14}\text{N} + ^{209}\text{Bi} \rightarrow ^{223}\text{Th}$	581
$^{16}\text{O} + ^{207}\text{Pb} \rightarrow ^{223}\text{Th}$	656

## Details of the Setup

MWPC	Folding Angle	Distance
MWPC 1	40°	23.5 cm
MWPC 2	122°	22.5 cm



## Experiment at JINR, Dubna for FFMD



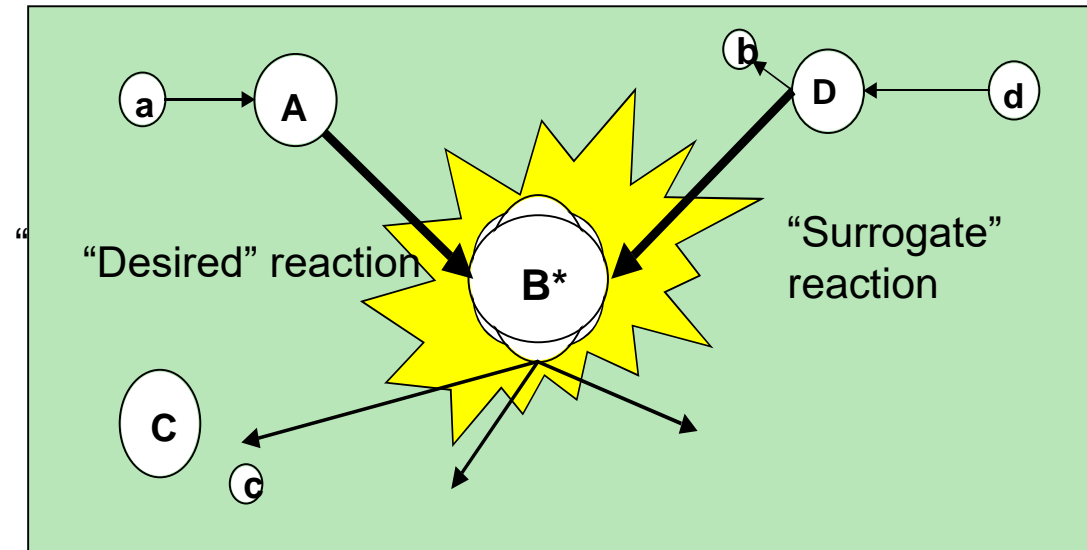
*By performing this, we can study change in the ground-state deformations of the  $^{222}\text{Th}$ ,  $^{223}\text{Th}$ ,  $^{224}\text{Th}$  isotopes.*

# Study of the surrogate ratio method by determination of $^{56}\text{Fe}$ (n,xp) cross sections

The cross section  $\sigma_{\alpha\chi}$  for the  
“desired” two-step reaction



can be determined indirectly  
with the Surrogate method.



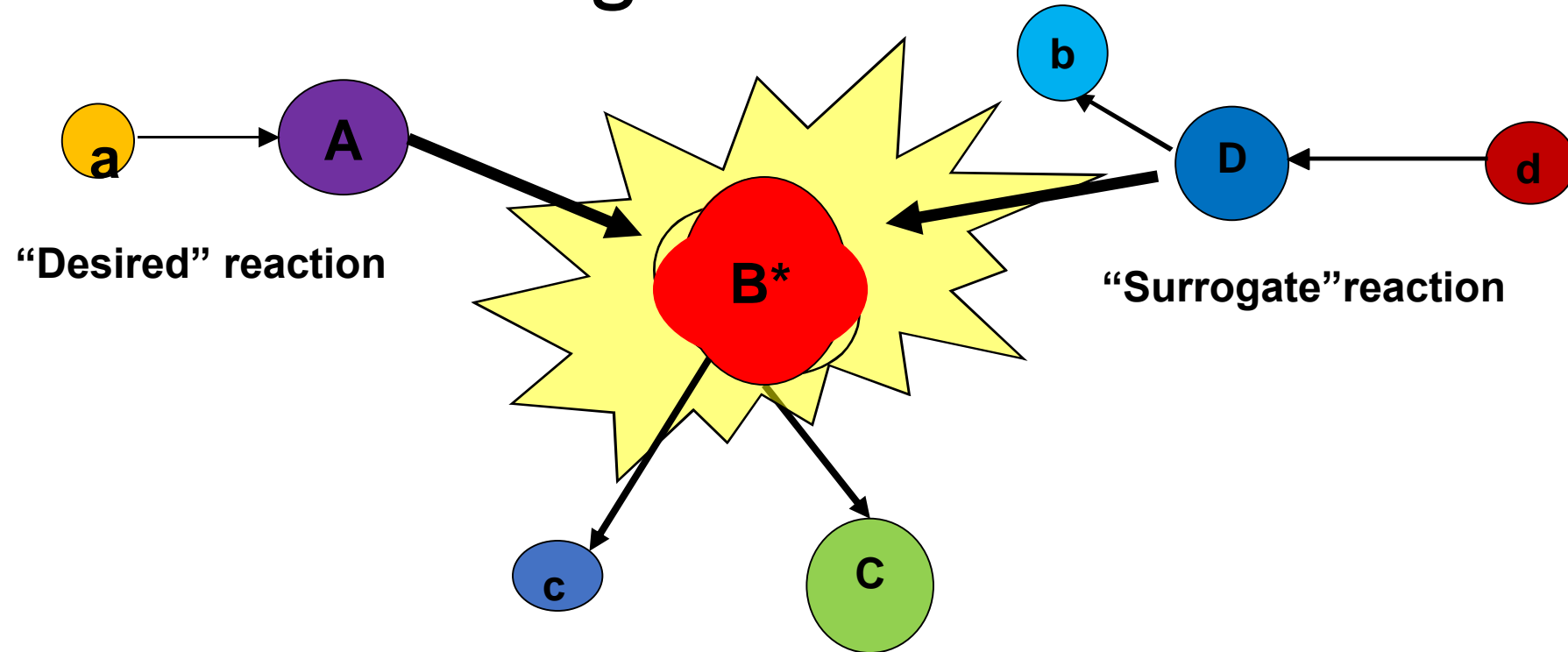
Form the compound nucleus  $B^*$   
via an alternative (“Surrogate”)  
reaction:



Then combine the measured  
decay probabilities for:

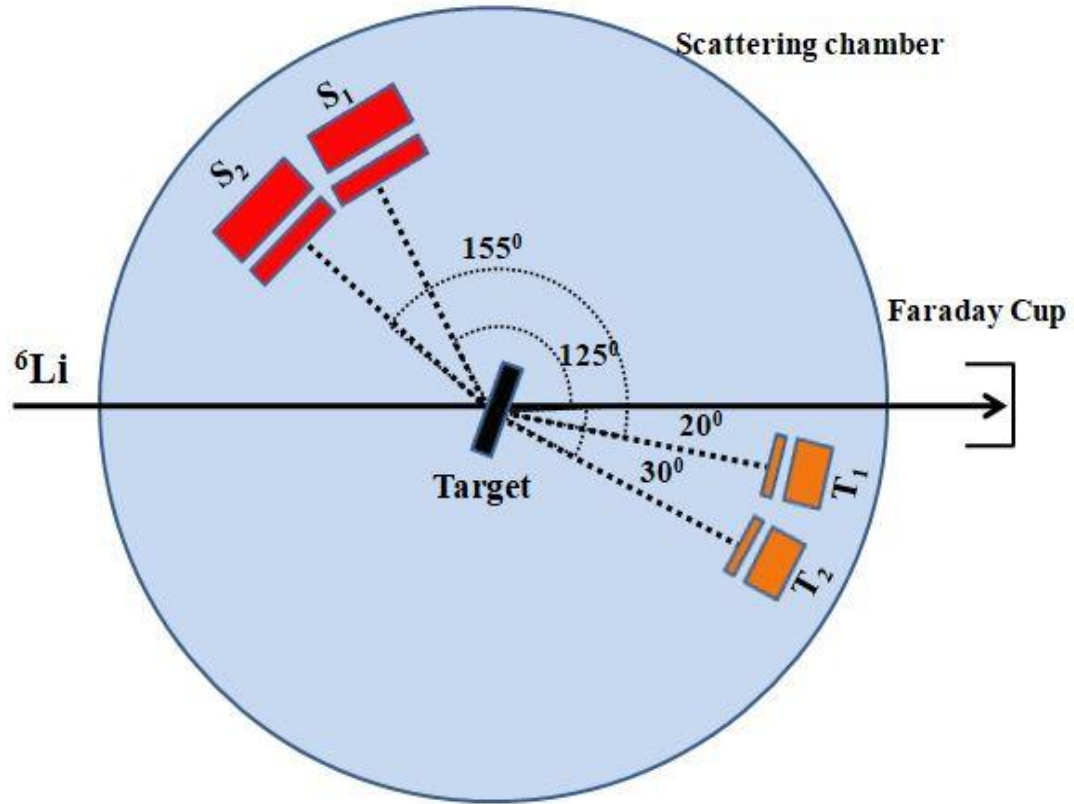


# Absolute surrogate method



$$\sigma_{A(a,c)C} = \sigma_{a+A}^{CN}(E_x) P_c(E_x)$$

# Requirements



## Chiba-Iwamoto condition

1. Spin of CN is less than  $10 \hbar$
2. Spin distribution of two reactions  $\rightarrow$  similar

# Methodology

Desired reaction:  $^{56}\text{Fe}(n, xp)$

Surrogate reaction:



$E(^6\text{Li}) = 25 \text{ MeV}$

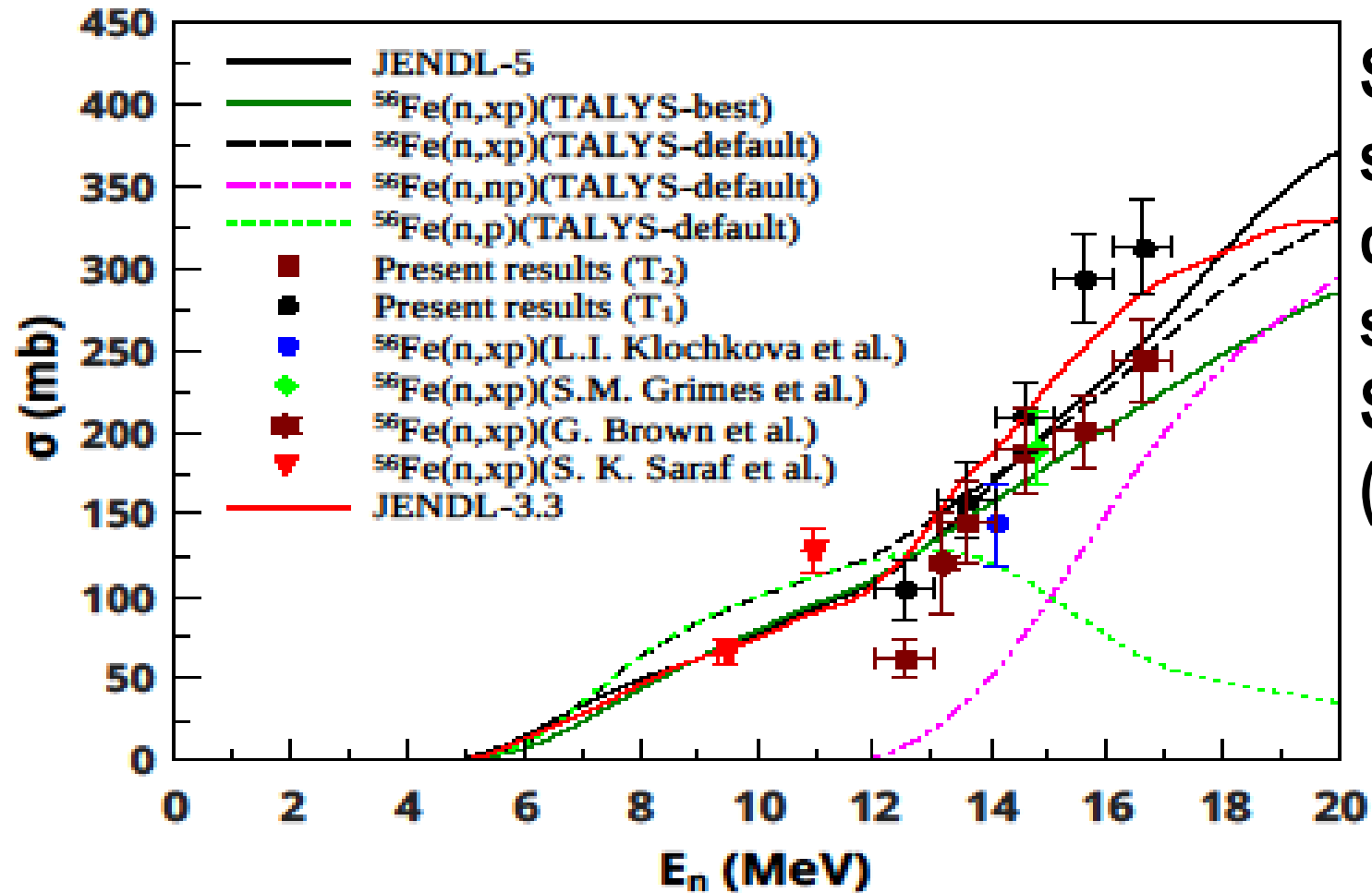
Reference reaction :  $^{52}\text{Cr}(n, p)$

Surrogate reaction:



$E(^6\text{Li}) = 25 \text{ MeV}$

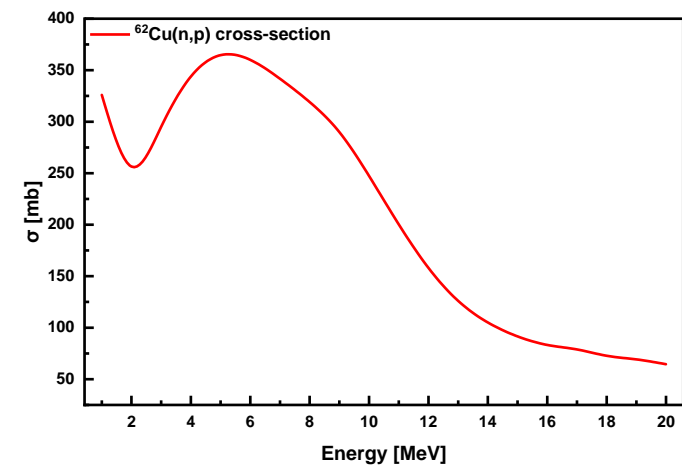
$$\frac{\sigma^{56\text{Fe}(n, xp)}(E^*)}{\sigma^{52\text{Cr}(n, xp)}(E^*)} = \frac{\sigma_{CN}^{n+56\text{Fe}}(E^*) P_{xp}^{57\text{Fe}}(E^*)}{\sigma_{CN}^{n+52\text{Cr}}(E^*) P_{xp}^{53\text{Cr}}(E^*)} \quad P_{xp}^{CN}(E^*) = \frac{N^{\alpha-p}(E^*)}{N^{\alpha}(E^*)}$$



**Study of the surrogate cross sections ratio method by determination of  $^{56}\text{Fe}(n,xp)$  cross sections, Ajay Tyagi, Aman Sharma et al, Phys Lett B 848, (2024)**

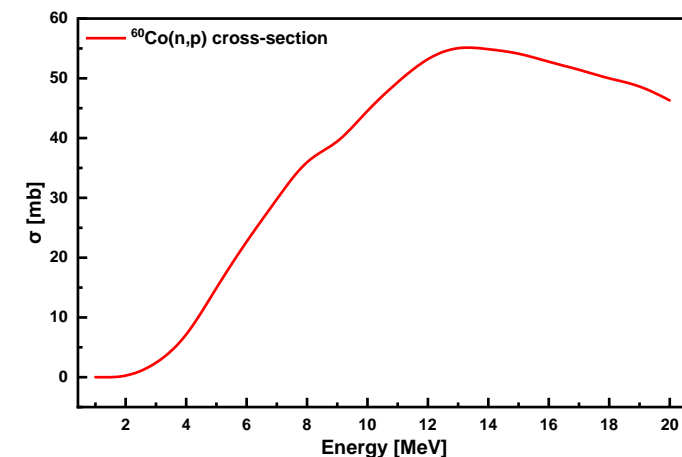
## Measurement of $^{62}\text{Cu}(n,xp)$ cross-section using surrogate ratio method:

<p>Desired Reactions: <math>^{62}\text{Cu}(n,xp)</math></p> <p>Surrogate Reaction:  <math>^7\text{Li} + ^{59}\text{Co} \rightarrow ^{63}\text{Cu} + t</math></p> <p><math>Q_{\text{gg}} = 3.307 \text{ MeV}</math>  <math>S_n = 8.875 \text{ MeV}</math>                      Excitation energy of CN equivalent to <math>E_n = 14 \text{ MeV}</math>  <math>E^* = 24.642 \text{ MeV}</math></p> <p>Using equation:  <math>E^* = Q_{\text{gg}} - Q_{\text{opt}}</math>  <math>E(^6\text{Li}) = 33.45 \text{ MeV}</math></p>	<p>Reference Reaction: <math>^{53}\text{Cr}(n,xp)</math></p> <p>Surrogate Reaction:  <math>^7\text{Li} + ^{51}\text{V} \rightarrow ^{54}\text{Cr} + \alpha</math></p> <p><math>Q_{\text{gg}} = 17.214 \text{ MeV}</math>  <math>S_n = 9.719 \text{ MeV}</math>                      For the excitation energy of CN = <math>24.642 \text{ MeV}</math></p> <p>Using equation:  <math>E^* = Q_{\text{gg}} - Q_{\text{opt}}</math>  <math>E(^6\text{Li}) = 19.85 \text{ MeV}</math></p>
---	--



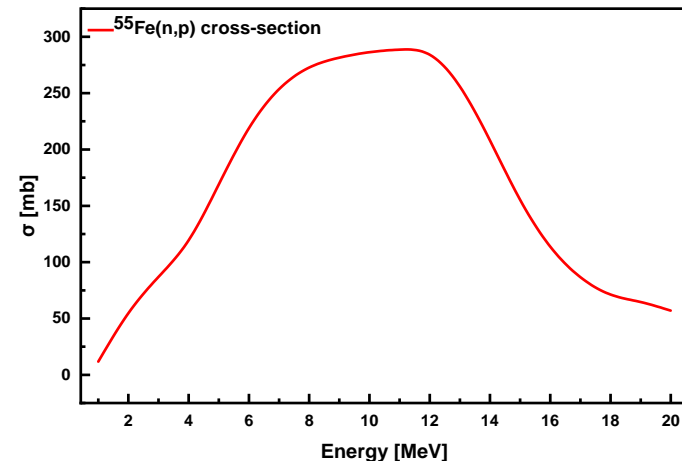
## Measurement of $^{60}\text{Co}(n,xp)$ cross-section using surrogate ratio method:

<p>Desired Reactions: <math>^{60}\text{Co}(n,xp)</math></p> <p>Surrogate Reaction:  <math>^7\text{Li} + ^{58}\text{Fe} \rightarrow ^{61}\text{Co} + \alpha</math></p> <p><math>Q_{\text{gg}} = 13.225 \text{ MeV}</math>  <math>S_n = 9.319 \text{ MeV}</math>                      Excitation energy of CN equivalent to <math>E_n = 14 \text{ MeV}</math>  <math>E^* = 23.089 \text{ MeV}</math></p> <p>Using equation:  <math>E^* = Q_{\text{gg}} - Q_{\text{opt}}</math>  <math>E(^7\text{Li}) = 35.8 \text{ MeV}</math></p>	<p>Reference Reaction: <math>^{61}\text{Ni}(n,xp)</math></p> <p>Surrogate Reaction:  <math>^7\text{Li} + ^{59}\text{Co} \rightarrow ^{62}\text{Ni} + \alpha</math></p> <p><math>Q_{\text{gg}} = 16.998 \text{ MeV}</math>  <math>S_n = 10.595 \text{ MeV}</math>                      For the excitation energy of CN = <math>23.089 \text{ MeV}</math></p> <p>Using equation:  <math>E^* = Q_{\text{gg}} - Q_{\text{opt}}</math>  <math>E(^7\text{Li}) = 48.382 \text{ MeV}</math></p>
--	---



## Measurement of $^{55}\text{Fe}(n,xp)$ cross-section using surrogate ratio method:

<p>Desired Reactions: <math>^{55}\text{Fe}(n,xp)</math></p> <p>Surrogate Reaction:  <math>^6\text{Li} + ^{52}\text{Cr} \rightarrow ^{56}\text{Fe} + d</math></p> <p><math>Q_{\text{gg}} = 6.138 \text{ MeV}</math>  <math>S_n = 11.197 \text{ MeV}</math>                      Excitation energy of CN equivalent to <math>E_n = 14 \text{ MeV}</math>  <math>E^* = 24.947 \text{ MeV}</math></p> <p>Using equation:  <math>E^* = Q_{\text{gg}} - Q_{\text{opt}}</math>  <math>E(^6\text{Li}) = 32.84 \text{ MeV}</math></p>	<p>Reference Reaction: <math>^{52}\text{Cr}(n,p)</math></p> <p>Surrogate Reaction:  <math>^6\text{Li} + ^{51}\text{V} \rightarrow ^{53}\text{Cr} + \alpha</math></p> <p><math>Q_{\text{gg}} = 14.746 \text{ MeV}</math>  <math>S_n = 7.939 \text{ MeV}</math>                      For the excitation energy of CN = <math>24.947 \text{ MeV}</math></p> <p>Using equation:  <math>E^* = Q_{\text{gg}} - Q_{\text{opt}}</math>  <math>E(^6\text{Li}) = 37.46 \text{ MeV}</math></p>
--	---



# Experimental work based on neutron induced reaction with different target material at Folded Tandem Ion Accelerator, BARC, Mumbai, India

$E_n$ (MeV)	Present data (mb)	Correlation matrix		
$1.67 \pm 0.14$	$10.8476 \pm 1.1544$	1.000		
$2.06 \pm 0.14$	$12.2408 \pm 0.9994$	0.1503	1.000	
$2.06 \pm 0.14$	$8.2430 \pm 0.7168$	0.1163	0.1587	1.000

1. Measurements of neutron capture cross sections on  $^{109}\text{Ag}$  at 0.53, 1.05, 1.66 MeV, M Upadhyay & **Ajay Kumar**. IEEE, 1-4, 2023.
2. Measurement of neutron induced reaction cross-section of  $^{99}\text{Mo}$ , M. Upadhyay & **Ajay Kumar**. Journal of Physics G: Nuclear and Particle Physics, (September 2023).
3. Neutron radiative capture cross section for sodium with covariance analysis, A. Gandhi & **Ajay Kumar**. The European Physical Journal A 57, 1 (2021).
4. Neutron capture reaction cross section measurement for iodine nucleus with detailed uncertainty quantification, A. Gandhi & **Ajay Kumar**. The European Physical Journal Plus 136, 819 (2021).
5. Measurement of neutron induced reaction cross-section of  $^{99}\text{Mo}$ , **Ajay Kumar** et al, Journal of Phys G, Oct 17, 2023

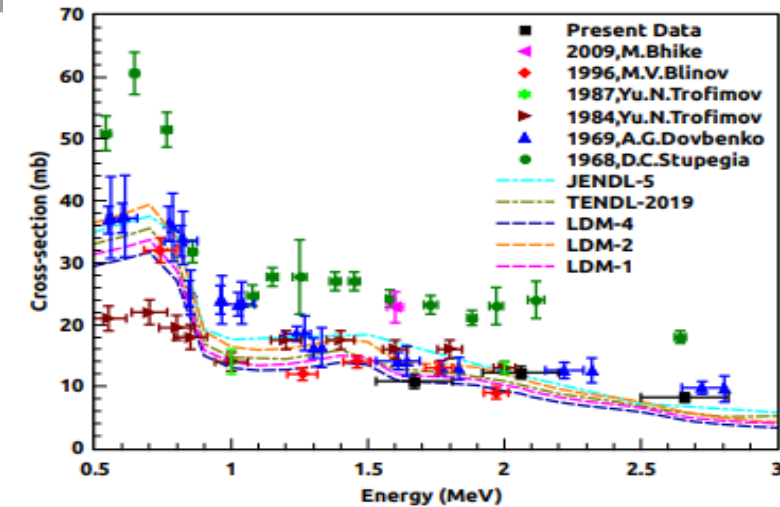


Fig.1 Cross-section of  $^{98}\text{Mo}(n,\gamma)^{99}\text{Mo}$  reaction measured in the present work compared with Exfor database, different level density models and different evaluated data libraries. (JPG, September, 2023)

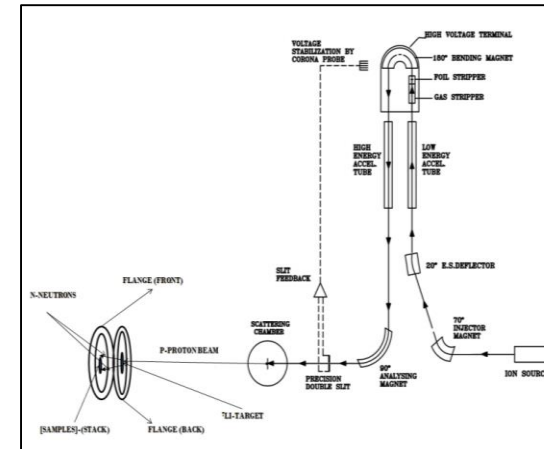


Fig. 2 FOTIA tandem accelerator (Experimental set up).



Fig. 3 Experimental set-up for the offline  $\gamma$ -ray spectroscopy using HPGe detector system.

# Experimental work based on alpha induced reaction with different targets at Variable Energy Cyclotron Center (VECC), Kolkata, India from 2022 to till now

Table.1

The calculated reaction cross-section, uncertainty and correlation matrix of the nuclear reaction  $^{nat}\text{Zn}(\alpha, x)^{65}\text{Zn}$ .

$E_\alpha$ (MeV)	Cross-section (mb) ( $\sigma \pm \Delta\sigma$ )	Correlation matrix																		
19.47 ± 1.15	1.78 ± 0.14	1																		
22.23 ± 0.98	20.74 ± 1.41	0.193	1																	
23.75 ± 1.09	27.01 ± 1.78	0.199	0.228	1																
26.18 ± 0.96	51.10 ± 2.99	0.224	0.257	0.265	1															
27.68 ± 0.89	51.49 ± 3.0	0.225	0.258	0.267	0.300	1														
29.75 ± 0.92	92.09 ± 5.44	0.222	0.255	0.263	0.296	0.297	1													
31.25 ± 0.52	99.27 ± 6.09	0.214	0.245	0.253	0.285	0.286	0.283	1												
33.15 ± 0.78	158.20 ± 9.63	0.216	0.247	0.255	0.287	0.288	0.285	0.274	1											
36.32 ± 0.46	278.78 ± 18.68	0.196	0.224	0.232	0.261	0.262	0.259	0.249	0.251	1										

1. Measurement of alpha-induced reaction cross-sections on  $^{nat}\text{Mo}$  with detailed covariance analysis, M Choudhary & Ajay Kumar. The European Physical Journal A 58(5), 1-10 (2022).
2. Measurement of excitation functions for  $^{nat}\text{Cu}(\alpha, x)$  reactions with detailed covariance analysis, M Choudhary & Ajay Kumar. Journal of Physics G: Nuclear and Particle Physics 50(1), 015103 (2022).
3. Measurement of alpha-induced reaction cross-sections for  $^{nat}\text{Zn}$  with detailed covariance analysis, M Choudhary & Ajay Tyagi. Nuclear Physics A 1038, 122720 (2023).
4. Excitation functions of alpha-particle induced nuclear reactions on  $^{nat}\text{Sn}$ , M Choudhary & Ajay Tyagi. Nuclear Physics A 1038, 122720 (2023).

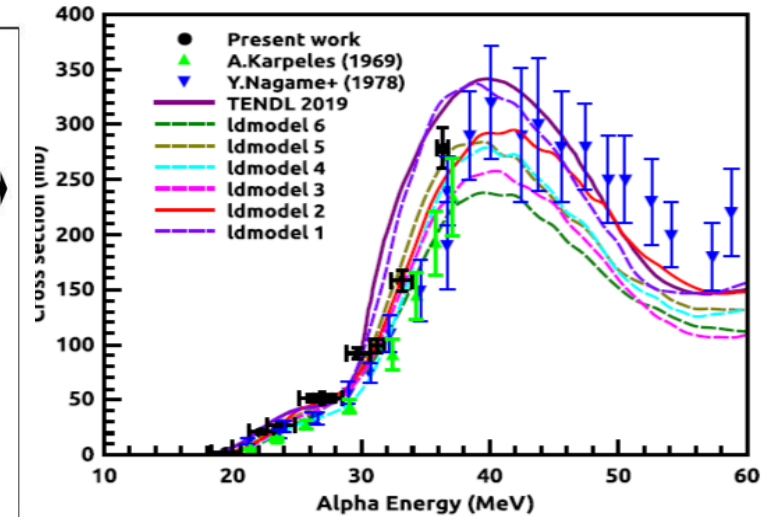
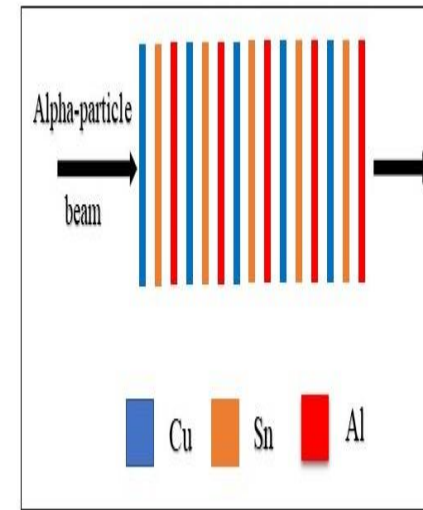


Fig.1 Cross sections for  $^{nat}\text{Zn}(\alpha, x)^{65}\text{Zn}$  reaction from this study in comparison of the available experimental data from EXFOR and theoretical calculation from TALYS. (Nuclear Physics A, 1038, 122720.)



Fig. 2 A close view photograph of the beam line

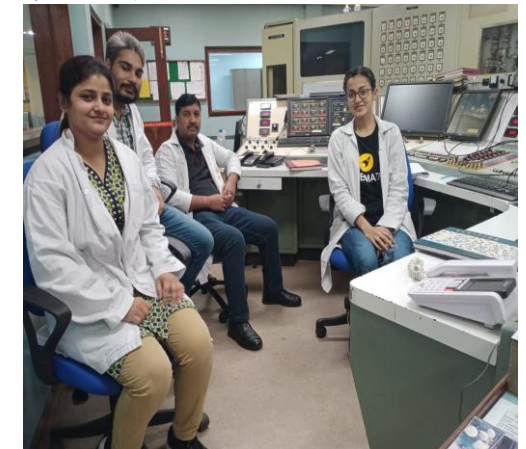


Fig. 3 A picture during the experiment at VECC, Kolkata, India

# Quasi-fission

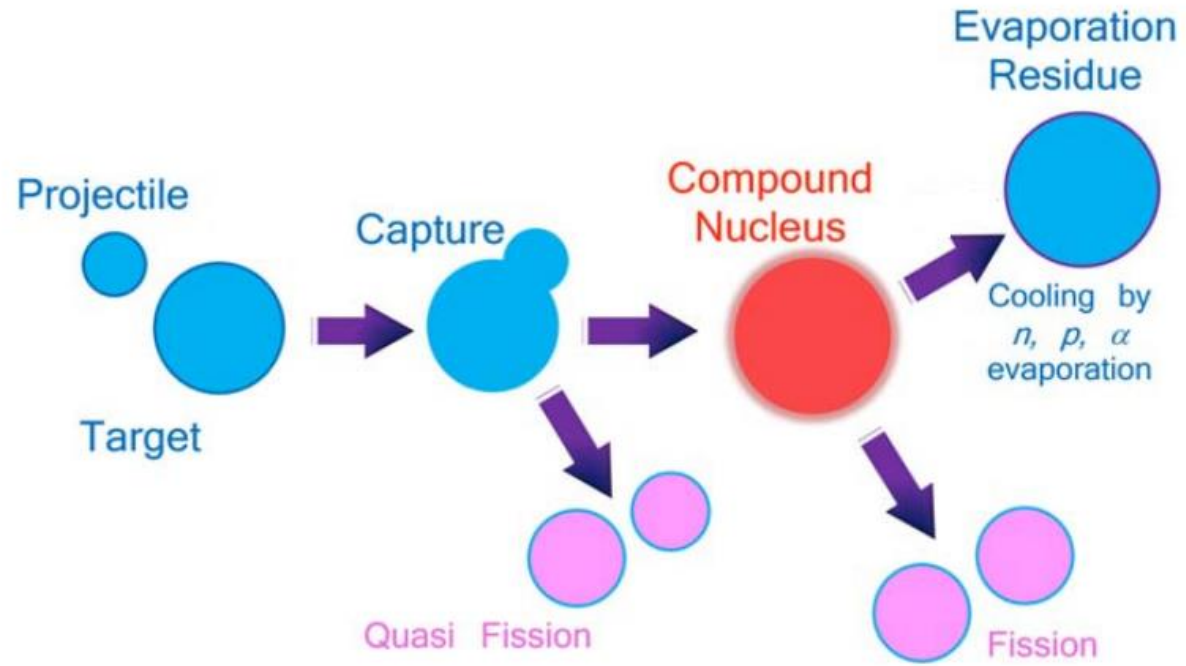


Figure: Schematic picture of different processes that occur in nuclear reactions

The main experimental challenge is to find the factors that prevent compound nucleus (CN) production. Measuring the parameters of the QF events can help with these factors. Also, no single parameter can establish quasi-fission with certainty. So, **we have accessed 41 nuclear reactions**, which are tabulated, along with the essential parameters that will help us to understand QF process thoroughly.

Then we have categorized these **reactions based on parameters**:

**Table: Role of high  $Z_P Z_T$  in quasi-fission.**

Sl. No.	Reaction	$Z_P Z_T$	$Z_T Z_P$	$\alpha$	$\alpha_{BG}$	$\chi_n$	Def. of projectile	Def. of target
1.	$^{86}\text{Kr} + ^{197}\text{Au}$	2844	43	0.392	0.943	0.937	0.000	-0.195
2.	$^{84}\text{Kr} + ^{198}\text{Pt}$	2808	42	0.404	0.940	0.906	0.086	-0.115
3.	$^{86}\text{Kr} + ^{198}\text{Pt}$	2808	42	0.394	0.939	0.900	0.000	-0.115
4.	$^{58}\text{Fe} + ^{208}\text{Pb}$	2132	56	0.564	0.927	0.796	0.259	0.000
5.	$^{40}\text{Ca} + ^{238}\text{U}$	1840	72	0.712	0.936	0.761	0.000	0.286
6.	$^{48}\text{Ca} + ^{208}\text{Pb}$	1640	62	0.625	0.909	0.676	0.000	0.000
7.	$^{40}\text{Ca} + ^{208}\text{Pb}$	1640	62	0.677	0.914	0.721	0.000	0.000
8.	$^{44}\text{Ca} + ^{198}\text{Pt}$	1560	58	0.636	0.900	0.681	0.000	-0.115
9.	$^{36}\text{S} + ^{238}\text{U}$	1472	76	0.737	0.925	0.647	0.168	0.286
10.	$^{32}\text{S} + ^{232}\text{Th}$	1440	74	0.75	0.921	0.669	0.208	0.207
11.	$^{34}\text{S} + ^{232}\text{Th}$	1440	74	0.744	0.896	0.654	-0.235	0.207
12.	$^{50}\text{Ca} + ^{176}\text{Yb}$	1400	50	0.557	0.761	0.619	0.000	0.289

Sl. No.	Reaction	CN	Barrier (MeV)	$Z_P Z_T$	$\alpha$	$\alpha_{BG}$	Def. of Projectile	Def. of Target
1.	$^{11}\text{B} + ^{235}\text{U}$	$^{246}\text{Bk}$	53.525	460	0.911	0.893	-	0.215
2.	$^{12}\text{C} + ^{178}\text{Hf}$	$^{190}\text{Pt}$	52.8036	432	0.874	0.816	--	0.278
3.	$^{12}\text{C} + ^{204}\text{Pb}$	$^{216}\text{Ra}$	58.8418	492	0.888	0.751	--	0.000
4.	$^{16}\text{O} + ^{175}\text{Lu}$	$^{191}\text{Au}$	68.544	568	0.832	0.823	-0.010	0.289
5.	$^{16}\text{O} + ^{186}\text{Os}$	$^{202}\text{Po}$	72.735	608	0.842	0.851	-0.010	0.209
6.	$^{14}\text{N} + ^{232}\text{Th}$	$^{246}\text{Bk}$	73.034	630	0.886	0.893	-	0.207
7.	$^{16}\text{O} + ^{209}\text{Bi}$	$^{225}\text{Pa}$	77.854	664	0.857	0.876	-0.010	-0.011
8.	$^{16}\text{O} + ^{232}\text{Th}$	$^{248}\text{Cf}$	82.8951	720	0.871	0.897	-0.010	0.207
9.	$^{16}\text{O} + ^{238}\text{U}$	$^{254}\text{Fm}$	84.369	736	0.874	0.902	-0.010	0.186
10.	$^{19}\text{F} + ^{232}\text{Th}$	$^{251}\text{Es}$	92.029	810	0.849	0.908	0.262	0.207
11.	$^{19}\text{F} + ^{238}\text{U}$	$^{257}\text{Md}$	93.6718	828	0.852	0.849	0.262	0.286
12.	$^{20}\text{Ne} + ^{205}\text{Tl}$	$^{225}\text{Pa}$	94.002	810	0.822	0.876	0.364	0.000
13.	$^{24}\text{Mg} + ^{186}\text{W}$	$^{210}\text{Rn}$	103.494	888	0.771	0.857	0.393	0.090
14.	$^{24}\text{Mg} + ^{178}\text{Hf}$	$^{202}\text{Po}$	101.475	864	0.762	0.851	0.353	-0.063
15.	$^{28}\text{Si} + ^{160}\text{Gd}$	$^{188}\text{Pt}$	105.619	896	0.702	0.818	-0.363	0.282
16.	$^{28}\text{Si} + ^{158}\text{Gd}$	$^{186}\text{Pt}$	105.905	896	0.698	0.821	0.218	0.282
17.	$^{30}\text{Si} + ^{176}\text{Yb}$	$^{206}\text{Po}$	112.781	980	0.708	0.846	-0.236	0.289
18.	$^{28}\text{Si} + ^{197}\text{Au}$	$^{225}\text{Np}$	126.558	1106	0.751	0.886	-0.363	-0.125
19.	$^{34}\text{S} + ^{168}\text{Er}$	$^{202}\text{Pb}$	125.13	1088	0.663	0.850	-0.235	0.297
20.	$^{32}\text{S} + ^{182}\text{W}$	$^{214}\text{Th}$	135.915	1184	0.701	0.878	0.208	0.232
22.	$^{34}\text{S} + ^{186}\text{W}$	$^{220}\text{Th}$	134.062	1184	0.691	0.873	-0.235	0.090
23.	$^{32}\text{S} + ^{232}\text{Th}$	$^{264}\text{Sg}$	158.959	1440	0.758	0.921	0.208	0.207
24.	$^{34}\text{S} + ^{232}\text{Th}$	$^{266}\text{Sg}$	157.585	1440	0.744	0.895	-0.235	0.207
25.	$^{36}\text{S} + ^{238}\text{U}$	$^{274}\text{Hs}$	159.125	1472	0.737	0.925	0.168	0.286
26.	$^{37}\text{Cl} + ^{154}\text{Sm}$	$^{191}\text{Au}$	121.625	1054	0.613	0.823	0.011	0.270
27.	$^{40}\text{Ca} + ^{154}\text{Sm}$	$^{194}\text{Pb}$	144.988	1240	0.587	0.884	0.000	0.270
28.	$^{48}\text{Ca} + ^{144}\text{Sm}$	$^{192}\text{Pb}$	141.065	1240	0.495	0.844	0.000	0.000
29.	$^{48}\text{Ca} + ^{154}\text{Sm}$	$^{202}\text{Pb}$	139.148	1240	0.525	0.836	0.000	0.270
30.	$^{48}\text{Ca} + ^{168}\text{Er}$	$^{216}\text{Ra}$	150.926	1360	0.555	0.751	0.000	0.297
31.	$^{48}\text{Ti} + ^{154}\text{Sm}$	$^{202}\text{Po}$	154.156	1364	0.527	0.850	0.011	0.272
32.	$^{50}\text{Ca} + ^{176}\text{Yb}$	$^{226}\text{Th}$	153.237	1400	0.557	0.761	0.000	0.289
33.	$^{50}\text{Ti} + ^{170}\text{Er}$	$^{220}\text{Th}$	165.736	1496	0.545	0.087	0.000	0.298
34.	$^{44}\text{Ca} + ^{198}\text{Pt}$	$^{242}\text{Cf}$	171.194	1560	0.636	0.900	0.000	-0.115
35.	$^{48}\text{Ca} + ^{208}\text{Pb}$	$^{256}\text{No}$	176.412	1640	0.625	0.909	0.000	0.000
36.	$^{40}\text{Ca} + ^{208}\text{Pb}$	$^{248}\text{No}$	181.325	1640	0.677	0.914	0.000	0.000
37.	$^{40}\text{Ca} + ^{238}\text{U}$	$^{278}\text{Cn}$	199.201	1840	0.712	0.936	0.000	0.286
38.	$^{58}\text{Fe} + ^{208}\text{Pb}$	$^{266}\text{Hs}$	227.209	2132	0.564	0.927	0.259	0.000
39.	$^{84}\text{Kr} + ^{198}\text{Pt}$	$^{282}\text{Fl}$	290.977	2808	0.404	0.940	0.086	-0.115
40.	$^{86}\text{Kr} + ^{198}\text{Pt}$	$^{284}\text{Fl}$	289.819	2808	0.394	0.939	0.000	-0.115
41.	$^{86}\text{Kr} + ^{197}\text{Au}$	$^{283}\text{Mc}$	294.151	2844	0.392	0.943	0.000	-0.195

From the above survey, we again re-tabulated them based on the deformation of the projectile and target.

**Table: Prolate-Prolate combination.**

SI No	Reaction	CN	$Z_p Z_T$	$Z_T - Z_p$	$\alpha$	$\alpha_{BG}$	$\chi_n$	Def. of projectile	Def. of target
1.	$^{12}\text{C}+^{232}\text{Th}$	$^{244}\text{Cm}$	540	84	0.901	0.890	0.389	--	0.205
2.	$^{14}\text{N}+^{232}\text{Th}$	$^{246}\text{Bk}$	630	83	0.886	0.893	0.425	-	0.207
3.	$^{19}\text{F}+^{232}\text{Th}$	$^{251}\text{Es}$	810	81	0.848	0.908	0.493	0.262	0.207
4.	$^{19}\text{F}+^{238}\text{U}$	$^{257}\text{Md}$	828	83	0.852	0.849	0.692	0.262	0.286
5.	$^{32}\text{S}+^{182}\text{W}$	$^{214}\text{Th}$	1184	58	0.701	0.878	0.612	0.208	0.232
6.	$^{32}\text{S}+^{232}\text{Th}$	$^{264}\text{Sg}$	1440	72	0.758	0.921	0.669	0.208	0.207
7.	$^{36}\text{S}+^{238}\text{U}$	$^{274}\text{Hs}$	1472	76	0.737	0.925	0.647	0.168	0.286
8.	$^{28}\text{Si}+^{158}\text{Gd}$	$^{186}\text{Pt}$	896	50	0.698	0.821	0.523	0.218	0.282
9.	$^{12}\text{C}+^{178}\text{Hf}$	$^{190}\text{Pt}$	432	66	0.874	0.816	0.353	--	0.278
10.	$^{11}\text{B}+^{235}\text{U}$	$^{246}\text{Bk}$	460	87	0.911	0.893	0.341	-	0.215

**Table: Spherical-Prolate combination.**

SI No	Reaction	CN	$Z_p Z_T$	$Z_T - Z_p$	$\alpha$	$\alpha_{BG}$	$\chi_n$	Def. of projectile	Def. of target
1.	$^{16}\text{O}+^{232}\text{Th}$	$^{248}\text{Cf}$	720	82	0.871	0.897	0.458	0.010	0.207
2.	$^{16}\text{O}+^{238}\text{U}$	$^{254}\text{Fm}$	736	84	0.874	0.902	0.462	0.010	0.186
3.	$^{37}\text{Cl}+^{154}\text{Sm}$	$^{191}\text{Au}$	1054	45	0.613	0.823	0.564	0.011	0.270
4.	$^{40}\text{Ca}+^{154}\text{Sm}$	$^{194}\text{Pb}$	1240	42	0.587	0.884	0.633	0.000	0.270
5.	$^{48}\text{Ca}+^{154}\text{Sm}$	$^{202}\text{Pb}$	1240	42	0.525	0.836	0.594	0.000	0.270
6.	$^{48}\text{Ca}+^{168}\text{Er}$	$^{216}\text{Ra}$	1360	48	0.555	0.751	0.621	0.000	0.297
7.	$^{48}\text{Ti}+^{154}\text{Sm}$	$^{202}\text{Po}$	1364	40	0.527	0.851	0.645	0.011	0.272
8.	$^{50}\text{Ca}+^{176}\text{Yb}$	$^{226}\text{Th}$	1400	50	0.556	0.761	0.619	0.000	0.289
9.	$^{50}\text{Ti}+^{170}\text{Er}$	$^{220}\text{Th}$	1496	46	0.545	0.870	0.664	0.000	0.298
10.	$^{40}\text{Ca}+^{238}\text{U}$	$^{278}\text{Cn}$	1840	72	0.712	0.936	0.761	0.000	0.286

**Table: Prolate-Spherical combination.**

SI No	Reaction	CN	$Z_p Z_T$	$Z_T - Z_p$	$\alpha$	$\alpha_{BG}$	$\chi_n$	Def. of projectile	Def. of target
1.	$^{58}\text{Fe}+^{208}\text{Pb}$	$^{266}\text{Hs}$	2132	56	0.564	0.937	0.796	0.259	0.000
2.	$^{20}\text{Ne}+^{205}\text{Tl}$	$^{225}\text{Pa}$	810	71	0.822	0.876	0.494	0.364	0.000

**Table: Prolate-Oblate combination.**

SI No	Reaction	CN	$Z_p Z_T$	$Z_T - Z_p$	$\alpha$	$\alpha_{BG}$	$\chi_n$	Def. of projectile	Def. of target
1.	$^{84}\text{Kr}+^{198}\text{Pt}$	$^{282}\text{Fl}$	2808	42	0.404	0.940	0.906	0.086	-0.115
2.	$^{24}\text{Mg}+^{178}\text{Hf}$	$^{202}\text{Po}$	864	60	0.762	0.851	0.518	0.353	-0.063

**Table: Spherical-Spherical combination**

SI No	Reaction	CN	$Z_p Z_T$	$Z_T - Z_p$	$\alpha$	$\alpha_{BG}$	$\chi_n$	Def. of projectile	Def. of target
1.	$^{48}\text{Ca}+^{208}\text{Pb}$	$^{256}\text{No}$	1640	62	0.625	0.909	0.676	0.000	0.000
2.	$^{40}\text{Ca}+^{208}\text{Pb}$	$^{248}\text{No}$	1640	62	0.677	0.914	0.721	0.000	0.000
3.	$^{48}\text{Ca}+^{144}\text{Sm}$	$^{192}\text{Pb}$	1240	42	0.495	0.844	0.599	0.000	0.000
4.	$^{12}\text{C}+^{204}\text{Pb}$	$^{216}\text{Ra}$	492	76	0.888	0.751	0.374	--	0.000

**Table: Spherical-Oblate combination**

SI No	Reaction	CN	$Z_p Z_T$	$Z_T - Z_p$	$\alpha$	$\alpha_{BG}$	$\chi_n$	Def. of projectile	Def. of target
1.	$^{44}\text{Ca}+^{198}\text{Pt}$	$^{242}\text{Cf}$	1560	58	0.636	0.900	0.681	0.000	-0.115
2.	$^{86}\text{Kr}+^{198}\text{Pt}$	$^{284}\text{Fl}$	2808	42	0.394	0.939	0.900	0.000	-0.115
3.	$^{86}\text{Kr}+^{197}\text{Au}$	$^{283}\text{Mc}$	2844	43	0.392	0.943	0.937	0.000	-0.195

**Table: Oblate-Prolate combination.**

SI No	Reaction	CN	$Z_p Z_T$	$Z_T - Z_p$	$\alpha$	$\alpha_{BG}$	$\chi_n$	Def. of projectile	Def. of target
1.	$^{28}\text{Si}+^{160}\text{Gd}$	$^{188}\text{Pt}$	896	50	0.702	0.818	0.532	-0.363	0.282
2.	$^{30}\text{Si}+^{176}\text{Yb}$	$^{206}\text{Po}$	980	56	0.708	0.847	0.526	-0.236	0.289
3.	$^{34}\text{S}+^{168}\text{Er}$	$^{202}\text{Po}$	1088	52	0.663	0.851	0.575	-0.235	0.297
4.	$^{34}\text{S}+^{186}\text{W}$	$^{220}\text{Th}$	1184	58	0.691	0.874	0.598	-0.235	0.090
5.	$^{34}\text{S}+^{232}\text{Th}$	$^{266}\text{Sg}$	1440	74	0.744	0.896	0.654	-0.235	0.207
6.	$^{16}\text{O}+^{175}\text{Lu}$	$^{191}\text{Au}$	568	63	0.832	0.823	0.412	-0.010	0.289

**Table: Oblate-Oblate combination.**

SI No	Reaction	CN	$Z_p Z_T$	$Z_T - Z_p$	$\alpha$	$\alpha_{BG}$	$\chi_n$	Def. of projectile	Def. of target
1.	$^{28}\text{Si}+^{197}\text{Au}$	$^{225}\text{Np}$	1106	65	0.751	0.886	0.587	-0.363	-0.125
2.	$^{16}\text{O}+^{209}\text{Bi}$	$^{225}\text{Pa}$	664	74	0.858	0.876	0.442	-0.010	-0.011
3.	$^{16}\text{O}+^{186}\text{Os}$	$^{202}\text{Po}$	608	68	0.842	0.851	0.425	-0.010	0.209

From the tables, we can ascertain that prolate-prolate and spherical-prolate combinations are the most probable ones for QF.

The figures give clear information about possible parameters that can cause the occurrence of quasi-fission.

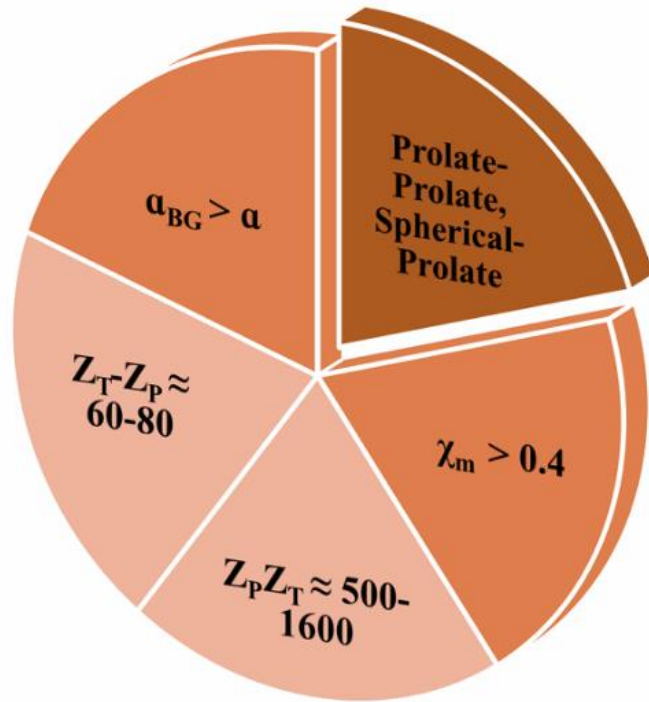


Figure: Representation of factors in favor of QF

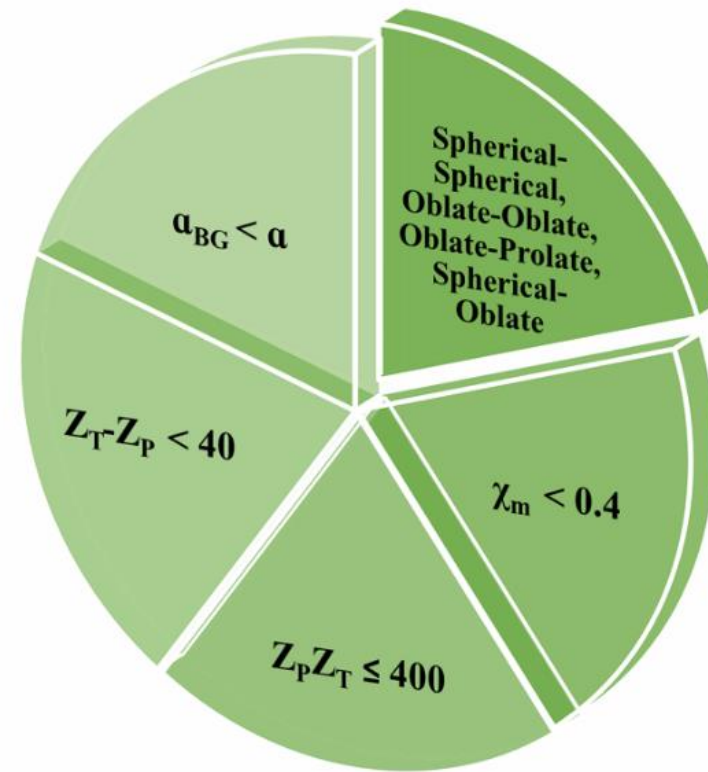


Figure: Representation of factors against QF

## A plan that can be executed abroad

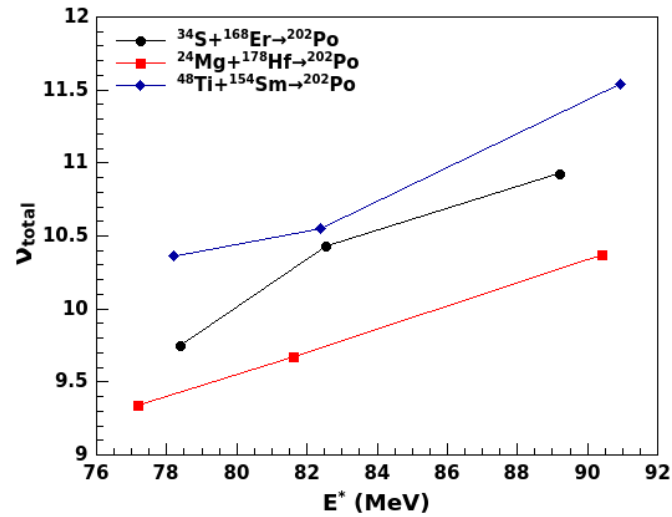


Figure: Theoretically calculated values of  $\nu_{total}$  with excitation energy for CN  $^{202}\text{Po}^*$

Table: Parameters of the reactions

Reaction	$Z_P Z_T$	$\alpha$	$\alpha_{BG}$	$\chi_m$	Def. of Target	Def. of Projectile
$^{34}\text{S} + ^{168}\text{Er}$	1088	0.6633	0.8505	0.6123	Prolate	Oblate
$^{48}\text{Ti} + ^{154}\text{Sm}$	1364	0.5274	0.8505	0.6641	Prolate	Prolate
$^{24}\text{Mg} + ^{178}\text{Hf}$ (unexpectedly lower value of $\nu$ , even no QF)	864	0.7623	0.8505	0.5692	Prolate	Prolate

Both  $^{34}\text{S} + ^{168}\text{Er}$  and  $^{48}\text{Ti} + ^{154}\text{Sm}$  reactions have high values of  $Z_P Z_T$  ( $< 1000$ ),  $\chi_m > 0.6$ , and a deformed target and projectile favouring QF. Whereas the  $^{24}\text{Mg} + ^{178}\text{Hf}$  reaction has lower values of  $Z_P Z_T$  and  $\chi_m$ , not supporting QF. So, the neutron multiplicity for  $^{24}\text{Mg} + ^{178}\text{Hf}$  should be higher than the other two reactions depicting QF. However, this is not the case, as shown in the figure above. The theoretically calculated values of neutron multiplicity for  $^{24}\text{Mg} + ^{178}\text{Hf}$  are significantly lower than those of the other two.

R. Rafiei *et al.*, Phys. Rev. C 77, 024606 (2008)

## A plan to be executed in India

Similar works have been proposed in VECC, Kolkata, to determine the probability of quasi-fission.

Table: Parameters of the reactions

Parameters	Reactions	
	$^{16}\text{O} + ^{169}\text{Tm} \rightarrow ^{185}\text{Ir}^*$	$^{16}\text{O} + ^{165}\text{Ho} \rightarrow ^{181}\text{Re}^*$
$Z_T - Z_P$	61	59
$Z_P Z_T$	552	536
$\alpha$	0.8270	0.8232
$\alpha_{BG}$	0.8128	0.7987
$\chi$	0.6630	0.6445
$\chi_m$	0.4073	0.4018
Def. Of Projectile	Spherical	Spherical
Def. Of Target	Prolate	Prolate

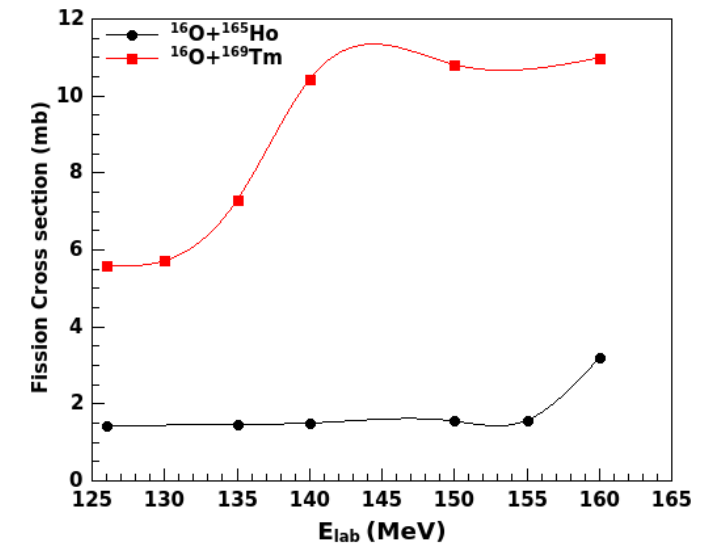


Figure: Theoretically calculated values fission cross section for both the nuclear reactions.

# DD based Neutron Generator at VDG, BHU

The neutron generator based on D-D nuclear reaction has been installed at VDG Building, Department of Physics, Banaras Hindu University, Varanasi.



Fig. A Picture of the D-D based Neutron Generator

Table: Major technical specifications of the Neutron Generator

DD neutron yield per pulse	$\geq 1 \times 10^9$ n/p (average)
Neutron energy (DD)	~2.5 MeV (typical)
Neutron pulse duration (FWHM)	~50 ns (typical)
Minimum time interval between shots	2 minutes (minimum)
Total energy stored	10 kJ (maximum)
Total capacitance	50 $\mu$ F (12.5 $\mu$ F $\times$ 4 Nos.)
Overall weight of system	300 kgs (approx.)
Overall size of the system	1.2 m x 0.9 m x 0.9 m



# Future Plans

1. To study the effect of shell closure in fusion-fission dynamics. ( at IUAC, New Delhi)
2. Study the effects of N/Z in heavy ion fusion-fission dynamics. ( at TIFR Mumbai)
3. Surrogate reactions a tool to study nuclear reactions without using neutrons. ( at IUAC, New Delhi)
4. Mapping of dissipation and entrance channel effects in heavy ion induced fusion reactions. ( at IUAC, New Delhi)
5. To determine the  $^{58}\text{Co}(n, p)$  cross section taking  $^{61}\text{Ni}(n, p)$  as the reference reaction using surrogate ratio method. ( at IUAC, New Delhi)

- **Indo Russian Bilateral research grant funded by DST-RFBR**
- **JINR, Dubna**
- **IUAC, New Delhi**
- **BARC, Mumbai**
- **TIFR, Mumbai**
- **VECC, Kolkata**

**Thanks**











( $d+D \rightarrow B^*+b \rightarrow c+C$ ), let  $\delta$  be the entrance channel ( $d+D$ ) of this reaction. The probability that the compound nucleus  $B^*$  is formed and decayed through desired exit channel  $\chi$  in a surrogate reaction, can be given using following equation.

$$P_{\delta\chi}(E^*) = \sum_{J\pi} F_{\delta}^{CN}(E^*, J, \pi) G_{\chi}^{CN}(E^*, J, \pi) \quad (3)$$

Where  $F_{\delta}^{CN}(E^*, J, \pi)$  is the formation probability of the desired compound nucleus ( $B^*$ ) in the surrogate reaction. The application of this method can be greatly simplified by using Weisskopf-Ewing approximation (35), which states that the branching ratios of the compound nucleus are spin and parity independent, therefore  $P_{\delta\chi}(E^*) = G_{\chi}^{CN}(E^*)$ ; since  $\sum_{J\pi} F_{\delta}^{CN}(E^*, J, \pi) = 1$  (9).  $P_{\delta\chi}(E^*)$  can be measured in a surrogate experiment by detecting the ejectile ( $b$ ) and decay particle ( $c$ ) in coincidence as  $P_{\delta\chi}(E^*) = \frac{N_{\delta\chi}}{N_{\delta}\epsilon_{\chi}}$ , where  $N_{\delta}$  is the total number of surrogate events, ( $N_{\delta\chi}$ ) is the number of coincidence counts  $b$  and  $c$ , and  $\epsilon_{\chi}$  is the detection efficiency of the particle  $c$  in the surrogate experiment. Using this decay probability the desired cross sections can be determined using following equation.

$$\sigma_{\alpha\chi}(E^*) = \sigma_{\alpha}^{CN}(E^*) P_{\delta\chi}^{CN}(E^*) \quad (4)$$

We will refer the above method in Eq. (4) as the ‘‘Weisskopf-Ewing’’ approximation in this manuscript. There is another